JOURNAL OF PETROLOGY | VOLUME 40 | NUMBER 5 | PAGES 679–704 | 1999

Cr-Pyrope Garnets in the Lithospheric Mantle. I. Compositional Systematics and Relations to Tectonic Setting

W. L. GRIFFIN[1,2]*, N. I. FISHER[1,3], J. FRIEDMAN[4], C. G. RYAN[1,2] AND S. Y. O'REILLY[1]

[1]ARC NATIONAL KEY CENTRE FOR GEOCHEMICAL EVOLUTION AND METALLOGENY OF CONTINENTS, DEPARTMENT OF EARTH AND PLANETARY SCIENCES, MACQUARIE UNIVERSITY, NSW 2109, AUSTRALIA

[2]CSIRO EXPLORATION AND MINING, PO BOX 136, NORTH RYDE, NSW 2113, AUSTRALIA

[3]CSIRO MATHEMATICAL AND INFORMATION SCIENCES, LOCKED BAG 17, NORTH RYDE, NSW 1670, AUSTRALIA

[4]DEPARTMENT OF STATISTICS, STANFORD UNIVERSITY, STANFORD, CA 91045, USA

RECEIVED JANUARY 12, 1998; REVISED TYPESCRIPT ACCEPTED OCTOBER 26, 1998

Chrome-pyrope garnet is a minor but widespread phase in ultramafic rocks of the continental lithosphere; its complex chemistry preserves a record of events related to fluid movements in the mantle, including melt extraction and metasomatism. We have examined the major-element and trace-element composition of >12 600 Cr-pyrope (Cr_2O_3 > 1 wt %) xenocrysts in volcanic rocks to evaluate their compositional ranges and interelement relationships. Samples have been divided into three major groups (Archon, ≥2·5 Ga; Proton, 2·5–1 Ga; Tecton, <1 Ga) depending on the age of the last major tectonothermal event in the crust penetrated by the host volcanic rock. Relative depths of garnets within each sample have been determined by measurement of Nickel Temperature (T_{Ni}). Mn, Ni and Zn contents of Cr-pyrope garnets are controlled by T*-dependent partitioning between garnet and mantle olivine. The expected correlation of* mg*-number with* T *is largely masked by effects of bulk composition and crystal chemistry. The Cr content of garnet is a primary indicator of the degree of depletion of the host rock; Fe, Y, Ti and Ga show negative correlations with Cr, suggesting that all have been removed as part of the primary depletion process. In garnets with T_{Ni} < 1200°C, the average degree of depletion as measured by these elements decreases from Archon to Proton to Tecton. High-temperature metasomatism, reflecting the introduction of asthenospheric melts, produces strong positive correlations between Fe, Zr, Ti, Y and Ga, and leads to 'refertilization' of previously depleted rocks. The prominent Ca–Cr correlation ('lherzolite trend') seen in garnets from clinopyroxene-bearing rocks is controlled primarily by the Cr/Al of the host rock, and Ca shows a strong negative association with Mg. The position and slope of the lherzolite trend vary with temperature and tectonic setting, suggesting that the* P/T *ratio exerts a control on Ca/Cr in lherzolite garnets. Garnets with less Ca than the lherzolite trend ('subcalcic garnets') are largely confined to Archon suites, where they typically are concentrated in the 130–180 km depth range. The few subcalcic garnets from Proton suites typically are lower in Cr and occur at shallower depths (100–120 km). Subcalcic garnets are absent in Tecton suites analysed in this work. The complexity of the geochemical relationships illustrated here, and their variation with temperature and tectonic setting, suggests that it is possible to define meaningful compositional populations of garnets, which can be used to map the stratigraphy and structure of the lithospheric mantle.*

KEY WORDS: *Cr-pyrope garnet*; *mantle*; *lithosphere*; *trace elements*; *kimberlite*; *lamproite*; *tectonothermal age*

INTRODUCTION

Knowledge of the composition of the subcontinental lithospheric mantle, and how that composition may have changed with time or tectonic setting, is essential to large-scale models of Earth's geochemical and tectonic

*Corresponding author.

evolution, and to the interpretation of seismic tomography. At present, the only means of studying the lithospheric mantle's composition directly is by analysis of xenolithic material in volcanic rocks. Boyd and coworkers, in a series of important papers (Boyd, 1989, 1997; Boyd & Mertzman 1987; Boyd *et al.*, 1993, 1997) have demonstrated that there are consistent differences in the bulk composition of mantle-derived ultramafic xenoliths, depending on whether those xenoliths are derived from ancient cratonic areas, or from regions with Phanerozoic crust. Griffin *et al.* (1998) examined the composition of Cr-pyrope garnet xenocrysts, representing fragments of mantle peridotite from a wide range of volcanic rock types, and found that the mean composition of such garnets varies systematically according to the tectonothermal age of the crust intruded by the host volcanic rock. This work defined major differences in mantle composition between regions with Archean crust and younger areas, and indicated an evolution toward less depleted average lithospheric compositions from ~2·5 Ga to the present.

These observations have important implications for Earth models: they suggest that lithospheric mantle is formed together with the overlying crust; that in most circumstances the lithospheric mantle (at least 200 km thick in Archean areas) and crust have remained coupled since formation, despite extensive plate-tectonic movements; and that replacement of older mantle by younger mantle of different composition, and hence different density, will have important tectonic consequences.

To learn more about lateral and temporal variations in the subcontinental lithosphere, we need tools for mapping mantle composition and structure over large areas. Xenolith suites in volcanic rocks can provide some of this information, but xenolith suites have major limitations for lithospheric mapping. The available xenolith record is strongly biased; it is dominated by samples from kimberlites penetrating Archean cratons, and from basalts erupted in areas of Phanerozoic tectonic activity. Few xenolith suites have been described from Proterozoic cratons, and many cratonic areas are represented very poorly, if at all, in the xenolith record (Nixon, 1987). It may also be difficult to obtain a representative picture of mantle composition beneath even a single area from xenoliths, simply for statistical reasons. Significant variation in lithology, both vertically and laterally, may exist beneath single volcanic fields (Griffin *et al.*, 1998, 1999*a*, 1999*b*), and individual eruptions may selectively sample different levels of the mantle section. This diversity means that very large numbers of xenoliths must be analysed from a single small area to provide a representative sample. After several decades of work by an army of researchers, this goal may have been achieved beneath parts of the Kaapvaal Craton, the Daldyn kimberlite field (more specifically, the Udachnaya pipe) in Yakutia, the Massif Central in France, and a small area of western Victoria in Australia. In other areas the xenolith record must be regarded as indicative, rather than representative.

A more widespread source of information exists in the xenocrystic minerals that can be separated from a wide range of mantle-derived volcanic rocks. Concentrates of these minerals provide a wider geographic and tectonic coverage than is possible from xenoliths alone. For example, Proterozoic cratons are represented in the published record only by two or three significant xenolith suites, e.g. Namibia (Hoal *et al.*, 1995) and Obnazhennaya, northern Siberia (Spetsius, 1995), whereas concentrates from over 100 localities in 16 distinct regions were available for this work (Appendix B). Xenocryst concentrates thus can provide data and insights difficult to obtain from the available xenolith suites. Concentrates also allow a statistical approach to analysing the lithological diversity of the lithospheric mantle. Each mineral grain in a concentrate may represent, in principle, a single xenolith, and it is feasible, both logistically and economically, to analyse hundreds of grains from a single volcanic field to obtain a representative sample.

Garnet concentrates in particular are a rich source of geochemical information, because of the wide range of composition (especially in trace elements) shown by this mineral (Griffin *et al.*, 1996*a*, 1996*b*, 1998; Schulze, 1995). Furthermore, the temperature of equilibration of a single garnet grain can be estimated from its Ni content (Ryan *et al.*, 1996). These temperatures can be used to place other geochemical information in a depth context, and thus to construct sections showing the vertical distribution of mantle lithologies and chemistry variables beneath each volcanic field for which samples are available (Griffin *et al.*, 1996*a*; O'Reilly & Griffin, 1996). This approach gives significantly more information than studies based on the simple relative abundances of different garnet types (Gurney & Zweistra, 1995; Schulze, 1995).

Where such sections can be compared with representative xenolith data and geophysical data, the results are in good agreement with major features represented in the xenolith suites (Griffin *et al.*, 1995, 1996*a*, 1999*b*). However, the more abundant data from the concentrates also have added information not available from the xenolith data. Griffin *et al.* (1995) and Brown *et al.* (1998) have used concentrate data to identify a major episode of lithosphere thinning and associated crustal uplift in the central Kaapvaal craton ~90 my ago; this was not recognized from xenolith studies because of the rarity of xenolith data from kimberlites with ages >90 Ma. In the Siberian craton, concentrate data have demonstrated that major structural and compositional features of the lithospheric mantle beneath the Daldyn field, well documented by xenolith studies, do not extend across nearby terrane boundaries mapped in crustal rocks (Griffin *et al.*, 1999*b*). This information was not obtainable from

xenolith suites because they are not available from the other kimberlite fields.

At present, lithosphere mapping by means of garnet concentrates is limited to the use of individual variables, or a few recognized metasomatic signatures (Griffin & Ryan, 1995; Griffin *et al.*, 1996*b*; O'Reilly & Griffin, 1996). The work reported here was initiated to investigate a more systematic use of garnet compositions to map the lithospheric mantle. We have analysed a large database of major- and trace-element data on mantle-derived Cr-pyrope garnets, from a wide variety of sources and tectonic environments. In this paper we examine some fundamental properties of this dataset, looking at the distribution of elements and inter-element correlations as a function of temperature, bulk composition and tectonic setting. We discuss the effects of crystal chemistry, phase equilibria and temperature on garnet composition, the nature and distribution of depletion (by melt extraction) and metasomatic processes, and variations in inferred bulk composition relative to tectonic setting and tectonothermal age of the mantle samples.

The emphasis in this paper is on the graphical illustration of major features and trends in the data, and interpretation of these in terms of major world-wide characteristics of the lithospheric mantle. We therefore do not attempt to provide regression lines, correlation matrices or other conventional statistical measures. In a companion paper, we will present a new analysis of compositional populations within this database, relate these populations to known xenolith types, and examine their stratigraphic distribution in lithospheric mantle of different age and from different tectonic environments.

DATABASE AND METHODS

The database used for this work (Appendix B) includes >13 000 analyses of individual grains of mantle-derived peridotitic garnet, defined by Cr_2O_3 contents $\geq 1\%$ and *mg*-number [Mg/(Mg + Fe)] >0·65. These garnets are assumed to have equilibrated with mantle olivine, thus allowing the application of the Nickel Thermometer described above. This coarse screen is necessary to pass the low-Cr garnets of many garnet peridotite xenoliths described from Tectons. It may also pass some garnets from Mg-rich pyroxenites or eclogites, but these appear to be very few, as will be seen below. The screen also allows the inclusion of many garnets of the 'megacryst' or 'discrete nodule' suite; these may be magmatic and their equilibration with olivine can be questioned. However, they typically give Nickel Temperature (T_{Ni}) >1200°C, suggesting equilibration with olivine at magmatic temperatures. Garnets with similar major- and trace-element characteristics, and similar high T_{Ni}, are common in high-T foliated xenoliths from kimberlites (Griffin *et al.*, 1989*b*; Smith *et al.*, 1991).

The data on these samples have been gathered largely through research done in support of the diamond exploration industry. Most analysed garnets were extracted from kimberlites, lamproites and other volcanic rocks; some samples are alluvial. The database contains samples from most continents, with a strong emphasis on southern Africa, Siberia, China, Canada and Australia; ~360 individual bodies from 226 localities in >30 major tectonic units are represented (Appendix B). Each record contains 15 compositional variables; other variables describe the tectonic setting, rock type, geographic position and economic value (diamond content) of the host rock.

Major- and minor-element data (Si, Ti, Al, Cr, Fe, Mn, Mg, Ca, Na) have been obtained by electron microprobe analysis (EMP), and trace elements (Ni, Zn, Ga, Sr, Y, Zr) by proton microprobe (PMP) analysis (Ryan *et al.*, 1990). The methods used impose constraints on the database. In many cases the Ti and Na values are below the EMP detection limits; the same is true for PMP data on Sr, and in some cases for Zr and Y. Distinction was made between values analysed but below detection, and missing values where elements were not analysed; the latter are rare in this dataset.

The classification by tectonic setting used here is modified from that of Janse (1994), as discussed by Griffin *et al.* (1998). It is based on the tectonothermal age of crustal blocks; this is defined as the age of the last major tectonic, magmatic or other thermal event. In this modified classification, 'Archons' were last strongly heated >2·5 Ga ago, 'Protons' between 2·5 and 1·0 Ga, and 'Tectons' <1 Ga before present. In general, Archons are characterized by thick lithosphere and low geothermal gradients, and Tectons by thin lithosphere and high geothermal gradients, with Protons lying between (Griffin *et al.*, 1998). The classification of each garnet grain as Archon, Proton or Tecton thus groups the samples into broad classes that represent combinations of age, lithosphere thickness, and geothermal gradient. Within this database, the sampling is biased toward garnets from Archons, with smaller numbers from Protons and Tectons (Appendix B). The relatively small size of the Tecton dataset is to some extent compensated for by its remarkable homogeneity world-wide, as will be discussed below.

The T dependence of Ni partitioning between garnet and olivine has been discussed in detail by Griffin *et al.* (1989*a*), Griffin & Ryan (1996) and Ryan *et al.* (1996). These studies could not identify any pressure or compositional control on the partitioning. The Ni content of mantle olivine varies little (mean 2900 $\pm$ 360 ppm; Ryan *et al.*, 1996; O'Reilly *et al.*, 1997) compared with the range of Ni variation in mantle garnet (10–130 ppm in the samples studied here). This situation allows the

estimation of temperature for individual grains of garnet (T_{Ni}), as applied in this work, with a precision on the order of ± 50°C (Ryan *et al.*, 1996). T_{Ni} is regarded as recording the ambient temperature of each garnet grain at the time that it was entrained in the host magma. The Nickel Thermometer as calibrated by Ryan *et al.* (1996) has been shown to reproduce the equilibration T of xenoliths, derived by conventional thermobarometry, to ± 50°C. An alternative calibration of the Nickel Thermometer by Canil (1994) is regarded as invalid (Griffin & Ryan, 1996), but its use would not materially affect the relationships described here. T can be converted to depth by reference to a geotherm that is known from xenolith studies, or derived directly from a garnet concentrate as described by Ryan *et al.* (1996).

Several types of graphical display are used to illustrate the relationships among the variables. Box plots of log-transformed data [$(\ln(x + 1)$; Fig. 1] show the spread of values for each variable, with median values, interquartile ranges, and 1·5 × interquartile ranges. These plots were initially used to eliminate samples that represented extreme outliers in one or more variables ($n = 367$). Most such samples could be ascribed to analytical or data-transcription errors; these data points are not included in the figures. Scatter-plots of element concentrations vs T_{Ni} (eg. Figs 2 and 3) are self-explanatory; these plots also are equivalent to plotting each variable against a logarithmic function of the Ni content. The chi-plot (Fisher & Switzer, 1985; see Appendix A) is a graphical method for assessing the relationship between two variables; it is especially useful when there is a large volume of data, with subtle but interesting intervariable associations, or several populations with different associations between variables. Rank correlation plots simply use the rank-order values of the variables, rather than the values themselves. A rank-order plot of two variables shows the tendency of one variable to increase (or decrease) as the other increases; it is not dominated by a few values in the extreme tails of the distributions of the variables. Such plots therefore are particularly useful in visualizing correlations and trends in distributions with long tails; such tails are a characteristic of this dataset (Fig. 1). Two-element plots of rank correlation and corresponding chi-plots (e.g. Fig. 4; see also Fig. 6, below) are used to examine the nature of correlations among compositional variables.

RESULTS

Distribution of individual variables

The ranges of some individual variables in the complete dataset (minus the outliers discussed above) are shown in Fig. 1. Most variables show skewed distribution of values. The tightest distributions are defined by FeO, MnO and MgO; these are constrained by partitioning with mantle olivine of relatively constant composition ($Fo_{86–94}$, MnO 800–1600 ppm; O'Reilly *et al.*, 1997). Cr_2O_3 shows a strong negative skewness, which is echoed to some extent by CaO. The relatively narrow interquartile range in CaO values reflects partitioning with clinopyroxene in lherzolitic assemblages; the tails to lower and higher values reflect the presence of garnets from harzburgitic and wehrlitic assemblages, respectively. The Zn values are positively skewed. The same is true of Sr, Zr and Y, but in all three cases the distribution at the low-concentration end is limited by the minimum detection limit (MDL) of the proton-probe data (typically 1–2 ppm; 95% confidence limit); many values for Sr, in particular, fall below the 95% confidence limit.

When the data are broken down by tectonic setting, significant differences appear for some elements (Table 1, Fig. 1). TiO_2 values from Archon suites show twice the spread of the data from Proton or Tecton suites. The median Cr_2O_3 content drops from 5·3% in Archon suites, to 4·1% in Proton suites and to 2·0% in Tecton suites, although there is no significant difference in median CaO, FeO, MgO or MnO contents. The median Y (and Y/Ga) more than doubles from Archon to Tecton suites, whereas median Zr drops by 30% and median Zr/Y drops by a factor of three. These observations confirm those made by Griffin *et al.* (1998) on a smaller group of localities.

The data for garnets from Tectons show less scatter in most individual variables than those for the Archon and Proton datasets (Fig. 1, Table 1). This is not simply a function of the smaller sample size, but reflects a remarkable similarity in the compositions of Tecton garnets, regardless of geographic location.

Distribution of elements relative to temperature

In Fig. 2, the concentrations of individual variables are plotted against temperature (T_{Ni}), estimated from the nickel content of each grain (Ryan *et al.*, 1996). Each plot includes a line representing a running smoothed average of the data at each T_{Ni}. In most tectonic situations T increases in a regular fashion with depth (the geotherm), though the detailed relationship varies from locality to locality. On a broad scale, T_{Ni} therefore serves as a proxy for depth. This relationship probably breaks down at some depth, where thermal aureoles around intrusive bodies of magma can provide a range of T at essentially constant depth. Many garnets with $T_{Ni} \geq 1200$°C may be derived from the wall-rocks of such thermal aureoles, or may be part of the common 'megacryst' or 'discrete nodule' population.

In these plots, monotonic variations of element concentration with T may reflect temperature-controlled

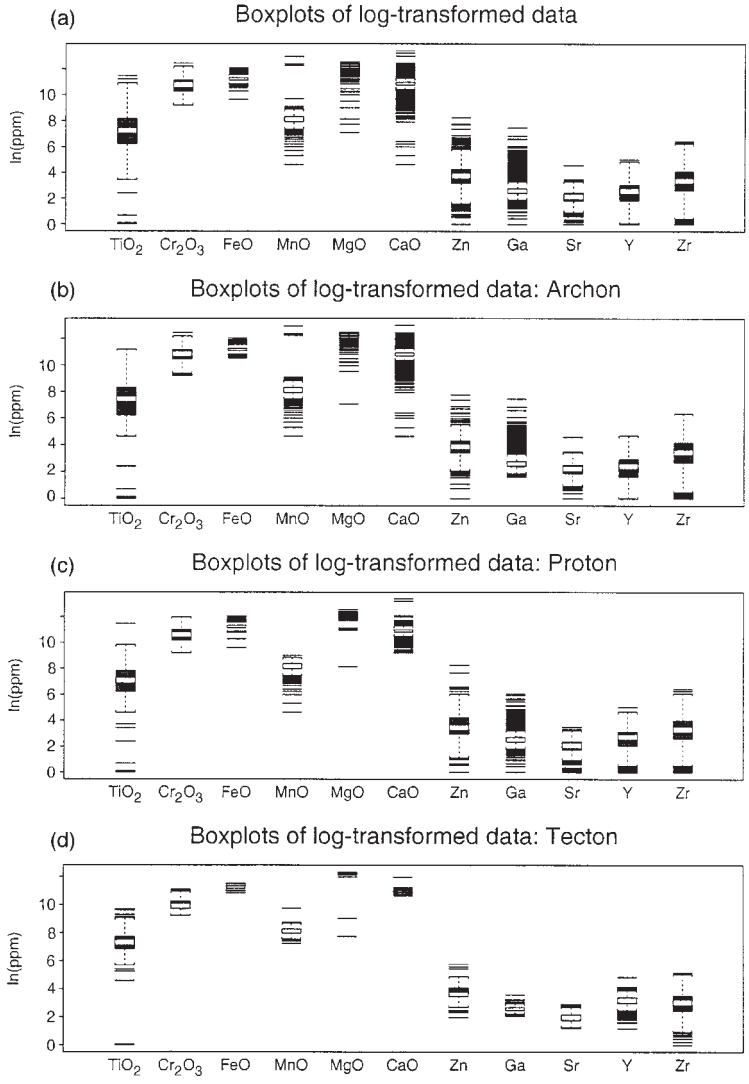

Fig. 1. Box-plots of log-transformed data [ln(x + 1)], showing median value, interquartile range (black box), and 1·5 × interquartile range (brackets). (a) All data; (b) Archons; (c) Protons; (d) Tectons.

variations in element partitioning between garnet and other phases. More complex variations may, in contrast, reflect variations in bulk composition, such as those caused by differences in degree of depletion, or by metasomatic processes.

In the complete dataset, average MgO increases regularly with T, as would be expected from the known partitioning between olivine and garnet (O'Neill & Wood, 1979). Mean FeO shows the corresponding decrease with increasing T, up to ~1100°C, and then levels out at higher T. Mean MnO decreases with increasing T, as noted by Smith *et al.* (1991), and mean Zn increases. TiO_2 increases markedly toward higher T, as does mean Zr (despite considerable scatter), whereas Sr, Y and Ga show more complex behaviour. Mean Cr rises up to ~1100°C, then falls. This effect is predicted by studies of the partitioning of Cr between garnet and chromite, which is sensitive to pressure (proxied here by T; Webb & Wood, 1986; Brey *et al.*, 1991; Ryan *et al.*, 1996).

When the data are divided by tectonic setting (Fig. 3), some interesting differences are observed. The average values of TiO_2 are similar at any T in all three groups, but the maximum TiO_2 at each T, especially in the main body of the data, is highest in Archons and lowest in Tectons. The maximum Cr_2O_3 content of garnet observed at any T, and the mean value at each T, differ among the three groups. In garnet sets from Archons, the maximum Cr and mean Cr rise more rapidly with

Table 1: Summary statistics for variables, by tectonic setting

	TiO_2 (ppm)	Cr_2O_3 (wt %)	FeO (wt %)	MnO (ppm)	MgO (wt %)	CaO (wt %)	Zn (ppm)	Ga (ppm)	Sr (ppm)	Y (ppm)	Zr (ppm)	*mg*-no.	Y/Ga	Zr/Y
Archon (n = *7478)*														
Upper quartile	4000	7·3	7·9	4000	21·1	5·7	15	11	2	17·5	63	84·8	1·8	6·0
Median	1700	5·3	7·2	3300	20·4	5·1	12	8	1	10·5	31	83·2	1·2	3·2
Lower quartile	500	3·5	6·6	2800	19·6	4·6	10	5·5	0·4	4	14	81·6	0·7	1·7
Proton (n = *4780)*														
Upper quartile	2500	6·0	8·4	4300	20·3	6	14	9·5	1·5	22	54	83·7	2·9	4·3
Median	1200	4·1	7·6	3600	19·7	5·4	12	7	1	14·5	27	82·2	1·8	2·2
Lower quartile	500	2·6	6·9	2900	19	5	10	5	0·1	7	13	80·5	1·1	1·0
Tecton (n = *422)*														
Upper quartile	2300	2·8	8·1	3900	20·8	5·5	14	7·5	1	29	33	83·7	5·0	1·4
Median	1500	2·0	7·7	3400	20·5	5·3	12	6	0·4	24	21	82·4	3·9	0·9
Lower quartile	960	1·7	7·1	2900	19·9	5·1	11	5	0	20	11	81·8	2·8	0·5
All (n = *12 680)*														
Upper quartile	3400	6·8	8·1	4100	20·9	5·8	15	10·5	2	20	59	84·3	2·3	5·2
Median	1400	4·7	7·4	3400	20·1	5·2	12	7·5	1	12·5	29	82·8	1·5	2·7
Lower quartile	500	3·0	6·8	2800	19·3	4·7	10	5	0·2	5·5	13	81·2	0·8	1·3

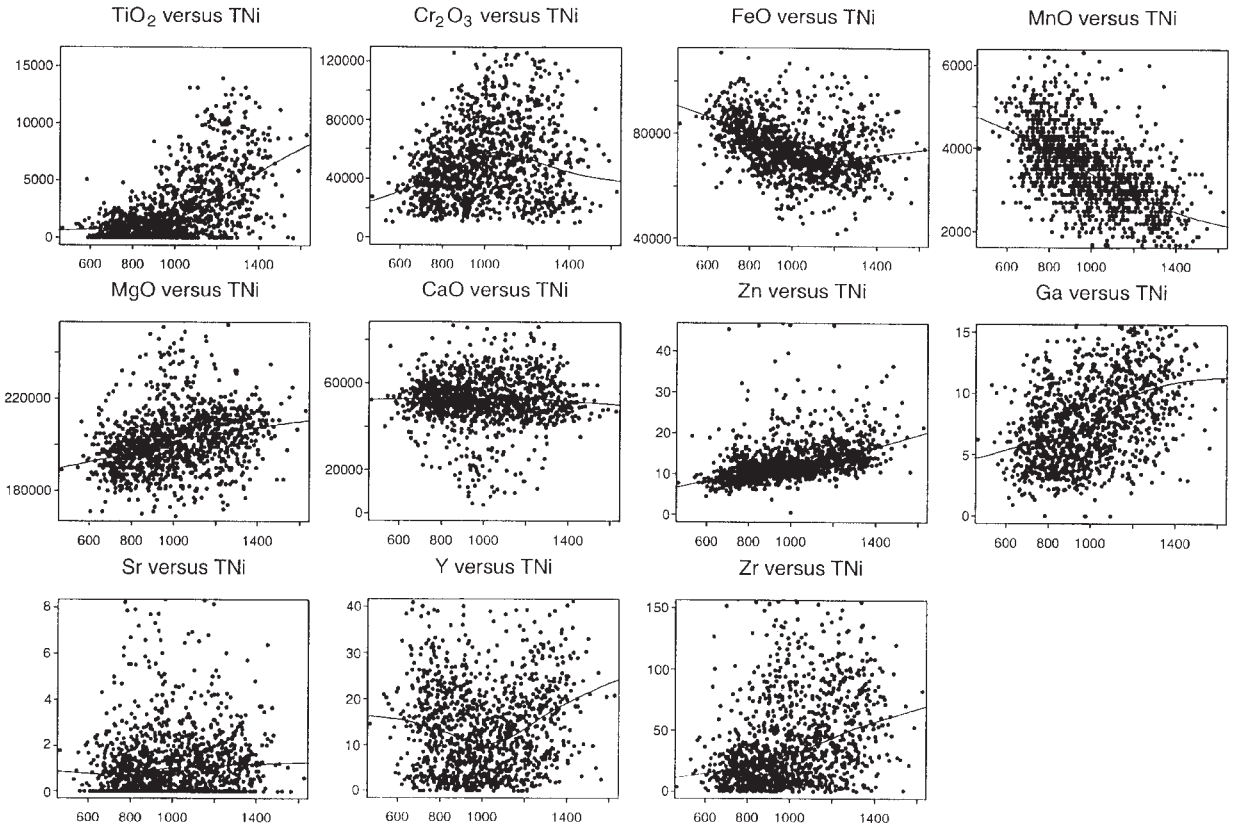

Fig. 2. Concentrations of individual elements plotted against Nickel Temperature (T_{Ni}, °C). A random 10% subset of the database is plotted; lines show smoothed average values at each T.

T, and the highest values are reached at lower T, than in the Proton datasets. The Tecton garnets rarely have >5% Cr_2O_3, and the maximum values are lower than in the other two classes except at the highest temperatures. Low-Ca, high-Mg garnets are common in Archon suites, and tend to concentrate at higher T than the few low-Ca garnets of Proton suites; these low-Ca garnets are absent in Tecton suites.

Sr contents ≥ 2 ppm are common in Archon suites, less so in Proton suites and rare in Tecton suites. There is a striking increase in mean Y content from Archon to Proton to Tecton, as noted above; this is especially true for garnets with $T_{Ni} < 1100$°C; in contrast, mean Ga contents tend to decrease in the same direction (Table 1). The mean Zr at each T is generally similar in Archon and Proton sets, but the mean Zr of Tecton garnets is significantly lower in the 800–1000°C range, where the data are concentrated. Zr/Y values >5 are common in Archon and Proton suites, but very rare in Tecton suites; the average Zr/Y decreases from Archon to Proton to Tecton (Table 1). The Y/Ga ratio is strongly T dependent in Archon and Proton garnet suites, with higher mean values at $T < 1000$°C. The mean Y/Ga at any T is lowest in Archon suites, and highest in Tecton suites (see Table 1).

The overall trends of MnO and Zn with temperature (not shown) are similar in all three tectonic groups, confirming that these are primarily T-controlled partitioning trends. All three groups show the same general pattern of declining FeO content with increasing T (Fig. 2).

Interelement correlations

Interelement correlations are illustrated by the use of rank correlation plots, linked with the corresponding chi-plots (Fig. 4). Several prominent associations are clearly linked to temperature-dependent partitioning between olivine and garnet; these include the negative correlations Mg–Fe, Zn–Mn and Mn–Mg, and the positive correlations Zn–Mg and Mn–Fe, which were noted above (Fig. 2). The strong positive correlation between Ca and Cr reflects the dominance of lherzolitic garnets (coexisting

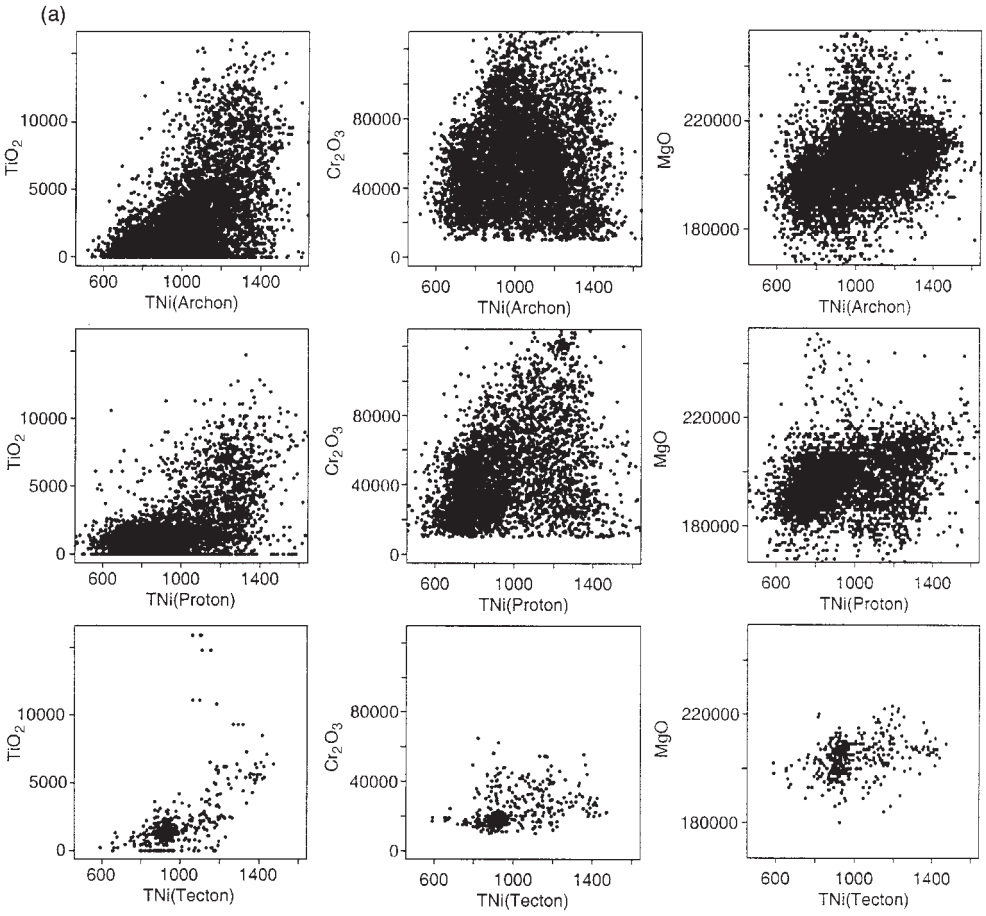

Fig. 3. (a).

with clinopyroxene) in the dataset (Fig. 5); the complexity in this association, illustrated by the diverging loops in the Ca–Cr chi-plot, arises from the presence of significant populations that lie to either side of the lherzolite trend. There is a strong negative association between Ca and Mg, and a much weaker one between Ca and Fe; these appear to be mainly a closure effect, reflecting the competition of these three major cations for the X site in the garnet structure. The plot of T_{Ni} vs Ca (Fig. 2), which shows no obvious correlation, demonstrates that the relation between Ca and Mg is not simply a temperature-related effect.

A number of elements, in addition to Ca, show marked associations with Cr_2O_3 content. Y and Fe show pronounced negative correlations with Cr. MgO is generally weakly negatively correlated with Cr, but the chi-plot shows that the Mg–Cr relationship is complex. Fe, Y, Zr, Ti, Zn and Ga are positively associated with one another, suggesting that these elements form a coherent group during depletion and enrichment processes in the mantle.

Interelement correlations vs temperature

Several of the interelement correlations visible in the complete dataset show marked variation with temperature. In Fig. 6a, selected elements are plotted against Cr_2O_3, for each temperature interval. At low T there is no clear association between Cr and Mg, but with increasing T (and mean Cr content) a strong negative correlation develops in high-Cr garnets; combined with the weak positive Cr–Mg association in low-Cr garnets, this gives a complex chi-plot. Y is negatively correlated with Cr at all T, but the relationship is simplest at low and high T. Ga and Ti (not shown) display no correlation with Cr at low T, but develop increasingly strong negative correlations with increasing T (and increasing mean Ti and Ga contents).

The positive correlations between Y, Fe, Zr and Ti, noted above, are present across the whole temperature range, but become especially pronounced toward high T (Fig. 6b). The Y–Zr association is most complex in the 900–1000°C range, which suggests that more than one process is involved.

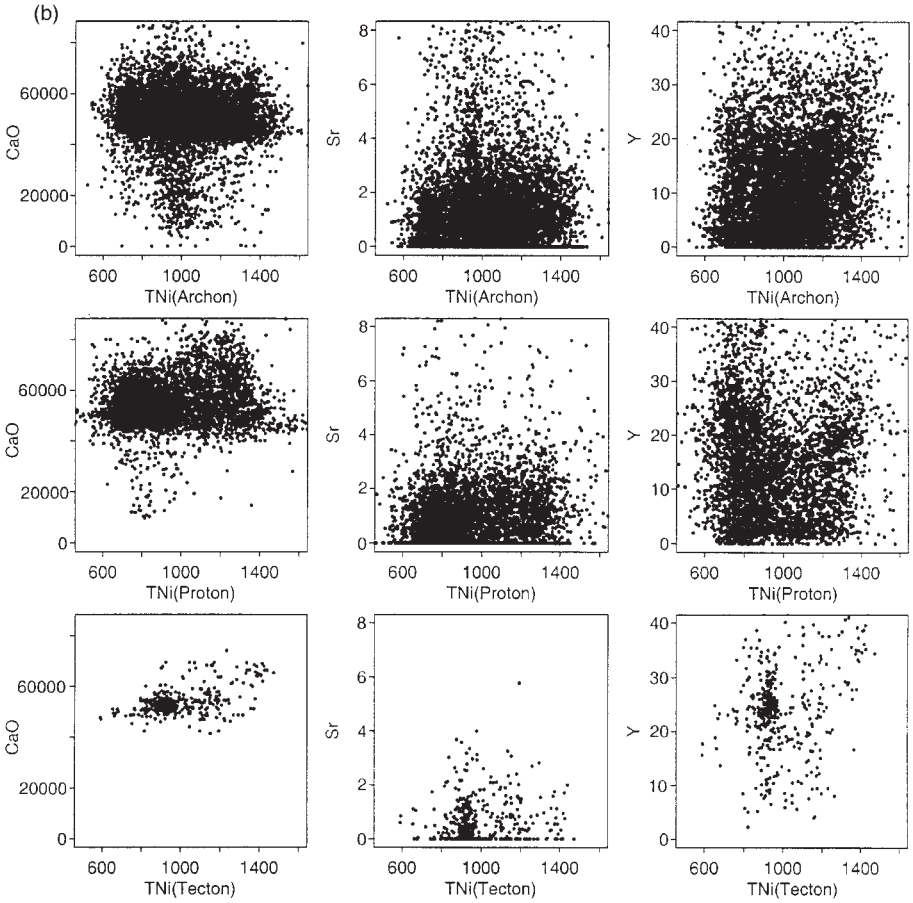

Fig. 3. (b).

Element correlations vs *T*: relation to tectonic setting

Several of the important interelement correlations described above, and their relation to temperature, vary significantly between suites from different tectonic settings (Archon, Proton, Tecton; Fig. 7).

The plots of CaO vs Cr_2O_3 (Fig. 7a) illustrate the scarcity of Ca-undersaturated garnets in Proton and Tecton suites, and the concentration of these garnets in the low-temperature ranges (<1100°C). The subcalcic garnets that are found in Proton suites are typically low in Cr_2O_3, though rare, high-Cr subcalcic garnets occur at high *T* in some Proton suites (see Fig. 5). The dominant lherzolite trend varies in position and slope between tectonic settings; these variations are discussed in detail below.

Cr and Mg are negatively correlated in low- and intermediate-*T* garnets from Archon suites (Fig. 7b), but at high *T* these suites contain an additional low-Cr population in which Cr and Mg are positively correlated. A similar pattern is seen in the Proton suites, but is less pronounced. In Tecton suites there is no correlation between Cr and Mg below 900°C, but a negative correlation at higher *T*. The negative correlation between Cr and Y (Fig. 7c) becomes more pronounced with increasing *T* in both Archon and Proton suites. It is well developed throughout the Tecton suites except at the highest *T*, but the slope of the trend is lower in Tecton suites than in the older ones. These plots also illustrate the general rise in mean Y contents from Archon to Tecton.

Figure 6b shows a good overall correlation of FeO with Y, but bifurcation in the chi-plot indicates a complex relationship. Figure 7d shows that some of this complexity is related to tectonic setting. In Archon suites, there is little correlation between Fe and Y at low *T*, but an increasingly good positive correlation toward high *T*. In contrast, in Proton suites the positive correlation is better developed at low *T* but becomes less pronounced as *T* increases.

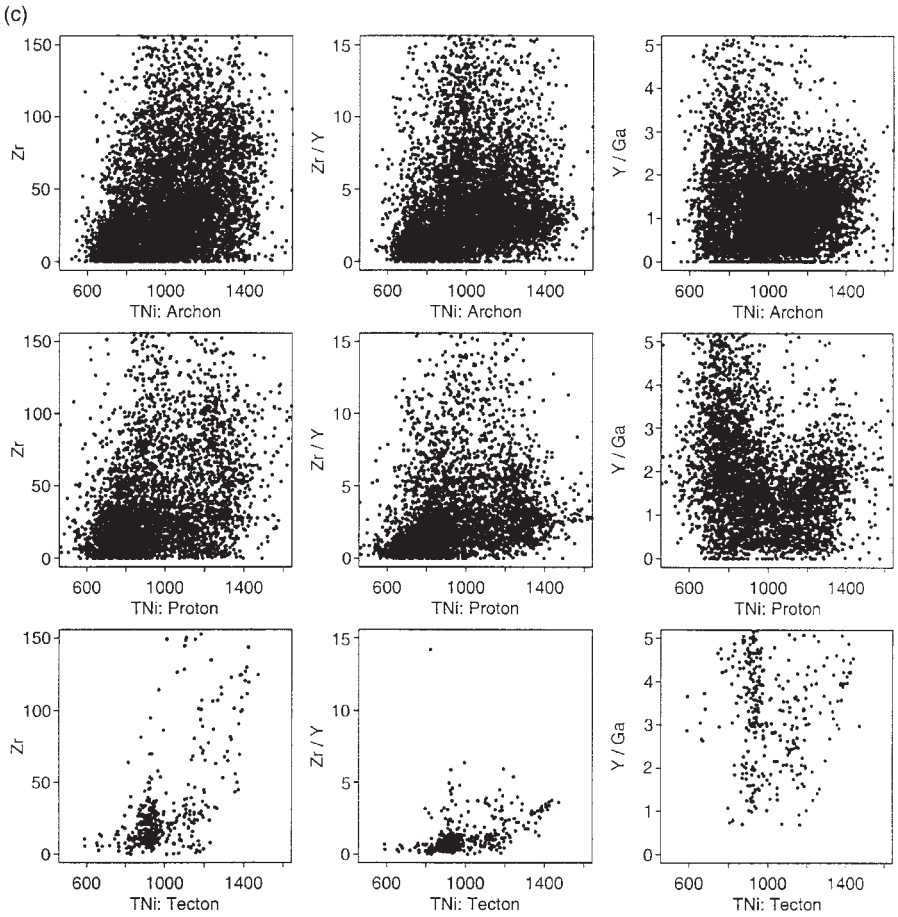

Fig. 3. Concentrations of individual elements plotted against Nickel Temperature (T_{Ni}), and divided by tectonic setting. (a) TiO_2, Cr_2O_3, MgO; (b) CaO, Sr, Y; (c) Zr; Zr/Y, Y/Ga.

Ti and Y are weakly correlated at low T in the Archon suites; as median Ti rises with increasing T, these two elements become increasingly well correlated (Fig. 7e). The same pattern is seen in the Proton and Tecton suites, and the mean Y/Ti ratio of the high-T garnets increases significantly from Archon to Proton to Tecton. Similarly, the mean Ga content and Ga/Y ratio (not shown) of Archon garnets increase with temperature, as these two elements become increasingly well correlated. The same is true of Proton suites, but the mean Ga/Y ratio of Proton garnets is lower for any Y content in each T interval. Tecton garnets show higher mean Y/Ga at all T (see Fig. 3; Table 1), but there is little correlation between Y and Ga except at high T. The mean Zr content, the mean Zr/Y ratio, and the degree of correlation between Zr and Y of Archon garnets also increase with T (Fig. 7f). In Proton and Tecton suites, Zr and Y are poorly correlated at low T but moderately well correlated for $T \geq 1000$°C. The mean Zr/Y at each T decreases from Archon to Proton to Tecton, for each T interval (see Fig. 3; Table 1).

DISCUSSION

The 'lherzolite trend'

The only patterns in these data that can be clearly ascribed to crystal-chemistry effects are those related to the known Ca–Cr correlation in lherzolitic garnets, which coexist with orthopyroxene and clinopyroxene and therefore may be regarded as Ca buffered (Fig. 5; Sobolev *et al.*, 1973; Gurney, 1984; Boyd *et al.*, 1993). This 'lherzolite trend' is one of the most pronounced correlations in this dataset, and is paralleled by a strong negative correlation between Ca and Mg (Fig. 5). We interpret these trends as primarily the result of a strong Ca–Cr interaction in the crystal lattice, as substitution of Cr for the larger Al ion allows the X site to expand (Smyth & Bish, 1988;

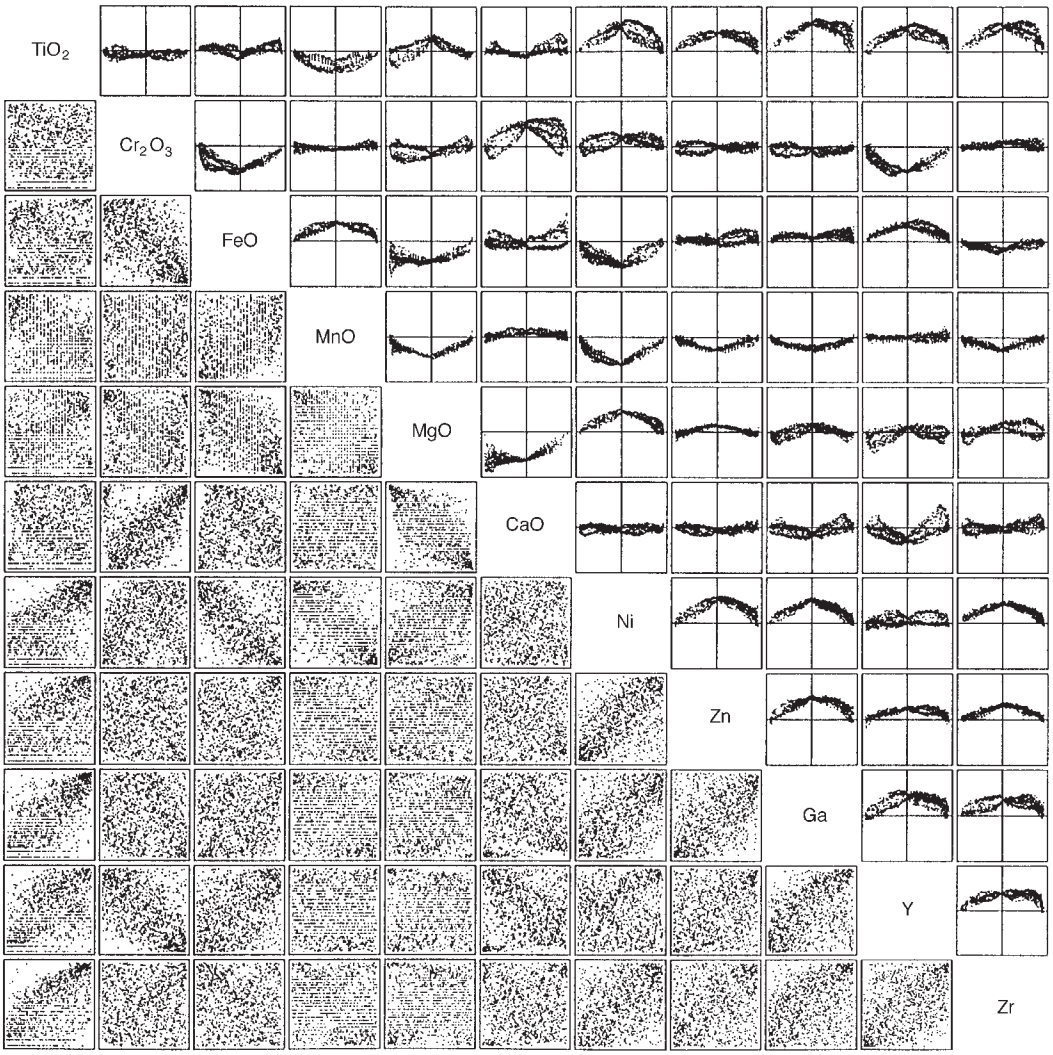

Fig. 4. Scatter plots of rank correlations for element pairs, with corresponding chi-plots (see Appendix A) illustrating interelement associations.

Smyth & McCormick, 1995), facilitating entry of the larger Ca ion.

The Cr content of the garnet closely reflects the Cr/Al of the rock, which is in turn a measure of the degree of depletion in basaltic components (Griffin *et al.*, 1998). As long as Ca is buffered by the presence of clinopyroxene, the Cr content will control the Ca content. The Mg and Fe contents of the garnet will reflect both the bulk composition of the rock and the effects of temperature. Higher Mg/Fe ratios are correlated with higher Cr/Al through the depletion process, and the Mg/Fe of garnet in equilibrium with olivine will rise with increasing T (O'Neill & Wood, 1979). The competition of Ca, Mg and Fe for the X site, coupled with the strong non-ideal interaction between Ca and Mg (Wood & Holloway, 1984) produces the negative correlations between Ca and Mg, and to a lesser extent Ca and Fe. The distribution of some minor and trace elements, such as Y and the rare earth elements (REE), may be influenced by the major-element composition of the garnets, as observed in eclogitic systems (O'Reilly & Griffin, 1995), but these relationships are not visible in our dataset.

The low-Ca side of the lherzolite trend is a matter of definition in Archon suites, but is obvious in Proton suites. The high-Ca side is well defined in both, and shows that the slope and position of the trend varies with tectonic setting, and with temperature (Figs 5 and 6a). At any T, the 'lherzolite trend' defined in this way lies at higher CaO in Tecton suites than in Proton or Archon suites, and the trend for Proton suites is consistently displaced to higher CaO at any Cr_2O_3, relative to the Archon suites. With increasing temperature the slope of

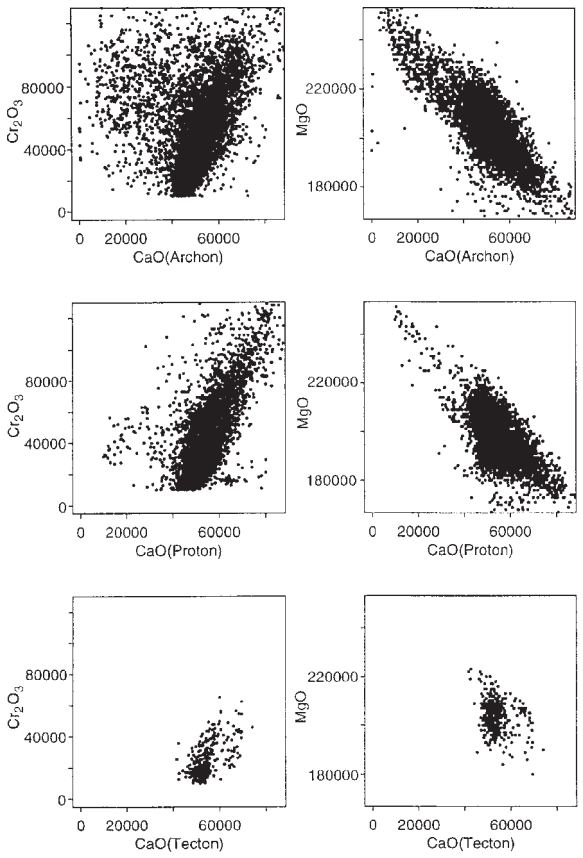

Fig. 5. Plots of Cr_2O_3 vs CaO and MgO vs CaO for data from each tectonic setting.

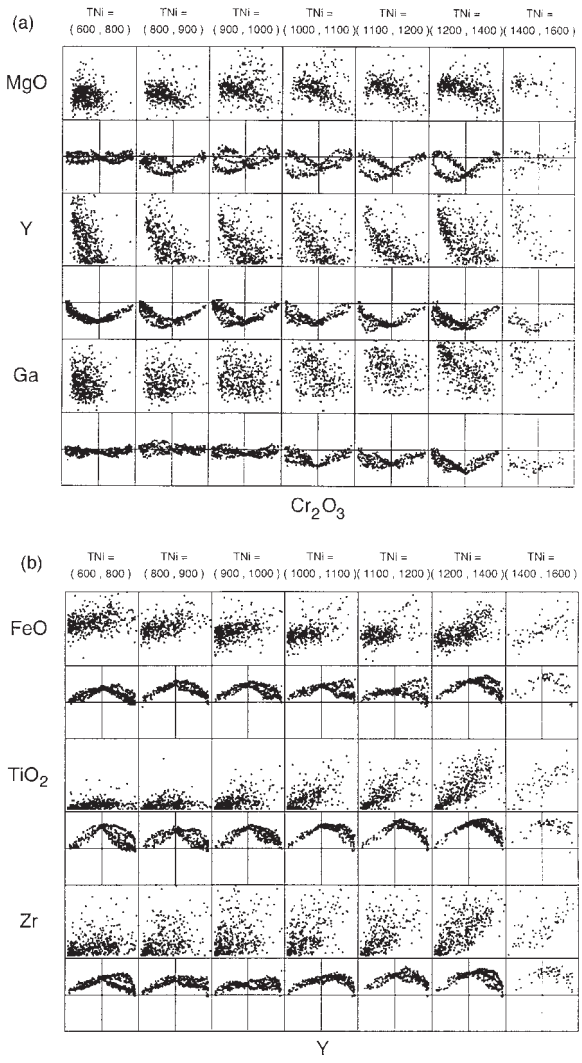

Fig. 6. Selected interelement correlations, with corresponding chi-plots, broken down by temperature interval. (a) Correlations with Cr_2O_3 (on abscissa); (b) correlations with Y (on abscissa). A random 10% subset of the database is plotted.

the trend becomes steeper (lower Ca/Cr) in Archon and Proton suites, but flatter (higher Ca/Cr at any Cr content) in Tecton suites.

The major difference between the different tectonic settings is in the lithospheric geotherm. Archons typically have low conductive geotherms, corresponding to low surface heat flow. The same is true of many Protons (Ryan *et al.*, 1996) but on average Proton geotherms are somewhat hotter (higher T at any P) than Archon geotherms. Tectons typically have higher surface heat flow (Morgan, 1995), reflecting elevated geotherms; in many cases these geotherms are strongly convex (high T at low P), indicating advective heat transport by magmas (O'Reilly & Griffin, 1985).

The differences in the slope and position of the lherzolite trend therefore are consistent with a pressure–temperature effect on the interaction between Cr and Ca in the garnet lattice, related to the increase in site radius required for Ca to enter the X site, as noted above. The increase in the slope of the trend with increasing T in Archon and Proton suites may reflect the rapid increase in P relative to T along the low conductive geotherms typical of cratonic areas, making the Ca substitution more difficult. In Tecton settings, where T increases rapidly relative to P (O'Reilly & Griffin, 1985), the slope of the lherzolite trend flattens with increasing T, as the lattice expands.

Brenker & Brey (1997) used experimental studies by Nickel (1983) and Brey (1989) to calibrate the variation of X_{Ca} of garnets in lherzolite assemblages, as a function of P and T. The experimental studies indicate that for a given Cr content (controlled by bulk composition) X_{Mg} increases and X_{Ca} decreases with increasing T and P. The P effect is marked from 2·5 to 4 GPa, but minor at

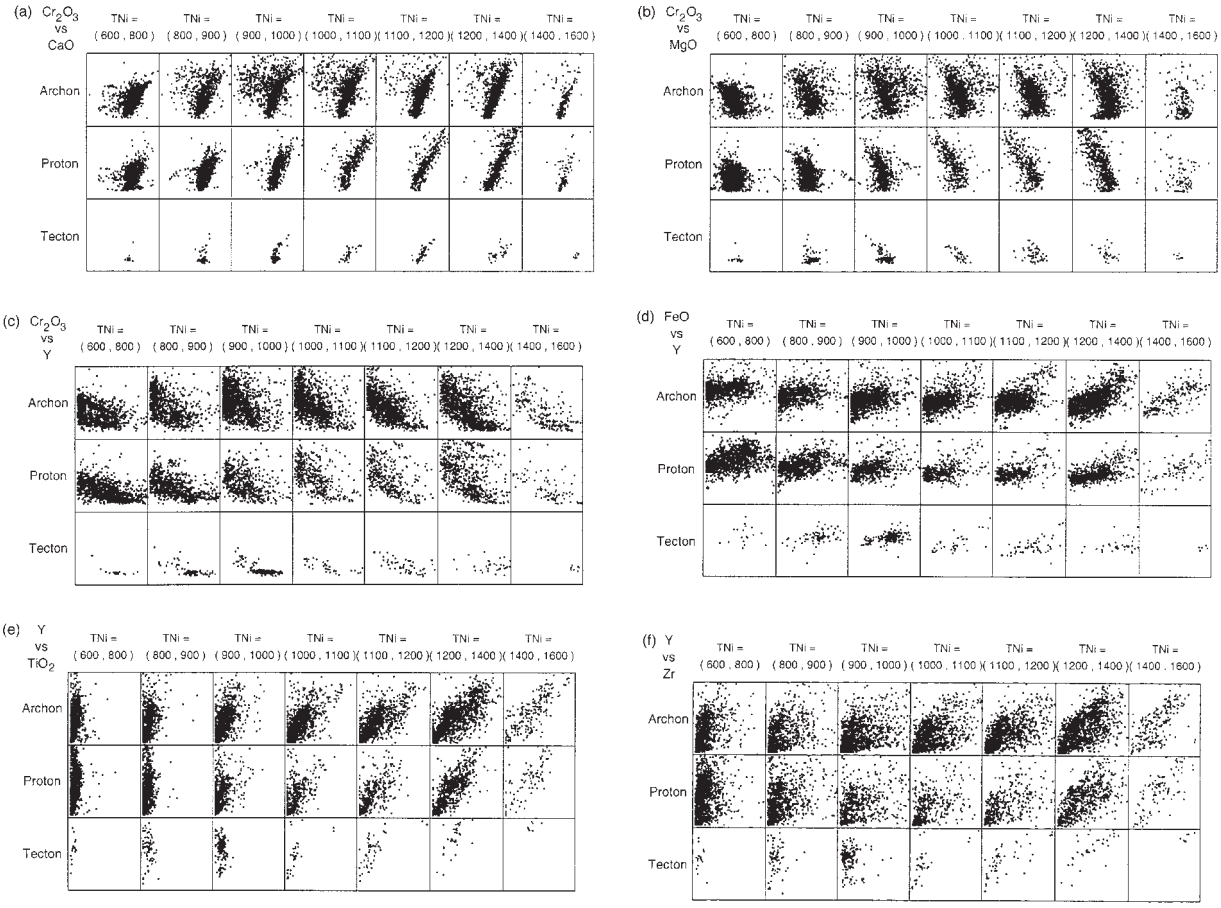

Fig. 7. Variation of selected interelement relationships with temperature, broken down by tectonic setting. (a) Cr_2O_3 (on ordinate) vs CaO; (b) Cr_2O_3 (on ordinate) vs MgO; (c) Cr_2O_3 (on ordinate) vs Y; (d) FeO (on ordinate) vs Y; (e) Y (on ordinate) vs TiO_2; (f) Y (on ordinate) vs Zr.

higher *P*. These observations are consistent with the patterns shown here. The Ca and Mg contents of garnets show a strong negative association in all three tectonic settings. CaO is essentially independent of *T*, whereas MgO increases with *T* up to ~1000°C, then tends to level out; 1000°C corresponds roughly to ~4 GPa on typical cratonic geotherms.

However, the high Ca and Ca/Cr of Tecton garnets, which are derived from areas with higher geotherms (higher *T* at any *P*) are not predicted by the experimental work. Brenker & Brey (1997) calculated an average slope for the lherzolite trend, which they 'assumed ... to be valid at any *P–T*', and this slope was used to calculate X_{Ca} as a function of X_{Cr}, *P* and *T*. As the data presented here show that the slope of the lherzolite trend varies with tectonic setting, and hence with the geotherm, the algorithm of Brenker & Brey (1997) should not be used to compare samples that may represent different *P–T* conditions.

Garnet data from the Colorado Plateau and the Jericho kimberlite in the Slave Province of Canada show two diverging 'lherzolite trends', corresponding roughly to the Tecton and Proton trends of Figs 5 and 7, and the flatter low-Cr trend is defined by garnets coexisting with Cr-rich spinel in lherzolitic parageneses (Smith *et al.*, 1991; Kopylova *et al.*, 1999). The apparent pressure–temperature effect on the lherzolite trend may therefore also reflect the wider stability field of gnt + spinel lherzolite assemblages in mantle sections with elevated geotherms. Webb & Wood (1986) demonstrated that the spinel + garnet field is broad in the fertile peridotites characteristic of Tecton settings, and narrower and deeper in the depleted compositions typical of Archon settings.

Temperature effects

A weak rise in MgO and decrease in FeO with increasing *T* is a feature of all garnet suites (Figs 2 and 3). This trend is generally expected in terms of the experimentally determined temperature dependence of Fe–Mg partitioning between garnet and mantle olivine (O'Neill &

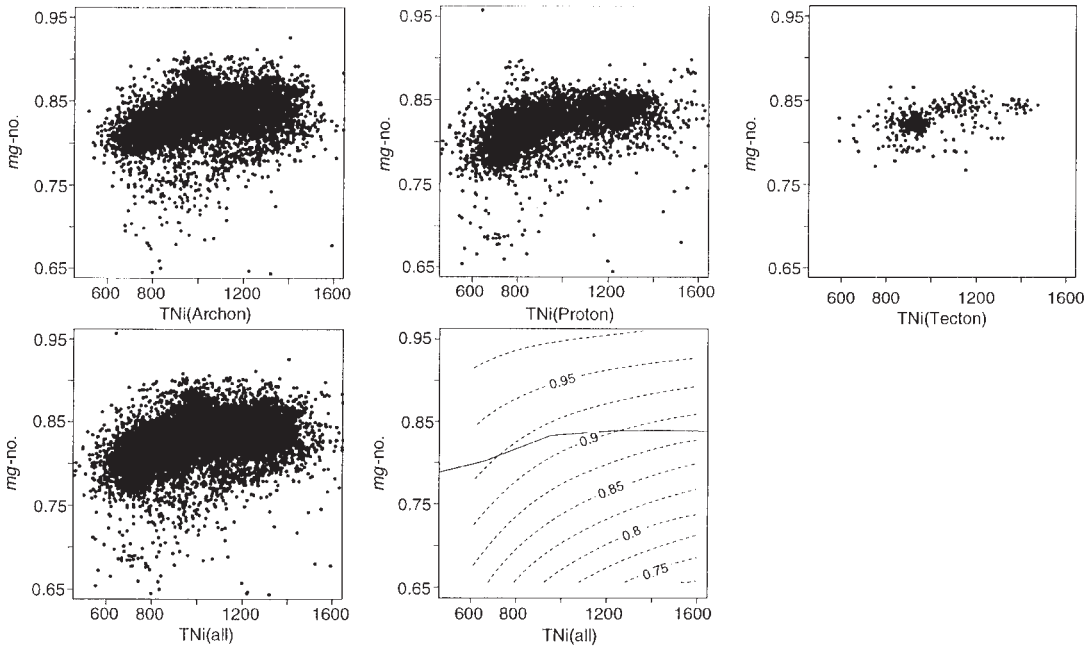

Fig. 8. *mg*-number [atomic Mg/(Mg + Fe)] of garnets vs temperature. Bold line shows smoothed average values of *mg*-number at each *T*. Dashed lines show trends expected for garnet equilibrated with olivine of a given *mg*-number, calculated using an inversion of the geothermometer of O'Neill & Wood (1979; Gaul *et al.*, in preparation).

Wood, 1979). A plot of *mg*-number [Mg/(Mg + Fe)] vs T_{Ni} for the whole dataset (Fig. 8) shows a gradual rise in *mg*-number with *T* up to ~1000°C, above which mean *mg*-number remains essentially constant. The observed range in *mg*-number of mantle olivine (0·86–0·94; O'Reilly *et al.*, 1997) is enough to produce most of the observed scatter in *mg*-number at each *T*. The few grains with *mg*-number lower than this range may be derived from magnesian, but olivine-free rocks such as pyroxenites or magnesian eclogites. Additional scatter is produced by the strong association between Ca and Mg, and its control by Cr content. At high *T* average garnet compositions are less magnesian than would be predicted by simple partitioning with a fixed average olivine composition over the whole *T* range (Fig. 8; see below). The boxplots of Fig. 1, and the plots in Fig. 3, show that the spread in MgO is greatest (at all *T*) in Archon suites; this reflects the presence in these suites of strongly depleted rocks with both magnesian olivine and low-Ca, high-Mg garnets.

The increase of Zn contents and decrease of Mn contents with increasing *T* are consistent in all garnet suites and appear to be independent of other compositional factors. For example, Fe and Zn are commonly correlated in minerals such as olivine (O'Reilly *et al.*, 1997), but in the garnet data this is not obvious (Fig. 4). Mn and Fe are positively correlated, but this may reflect their mutual relation to *T*, rather than a compositional dependence. The contents of both elements in garnet probably are controlled by partitioning between garnet and mantle olivine, which represents the major reservoir for these elements in ultramafic rocks. The mean Mn content of olivine from garnet peridotites is 795 $\pm$ 190 ppm and the mean Zn content is 55 $\pm$ 5 ppm (O'Reilly *et al.*, 1997). Smith *et al.* (1991) observed that Mn partitioning between garnet and olivine could be useful as a geothermometer, and is potentially more sensitive than Fe–Mg partitioning because of the greater range of variation relative to the precision of available analytical methods. The strong positive correlation of Zn with Ni, seen in the garnets, is the opposite of that found in coexisting chromites, where Zn decreases and Ni increases with increasing *T* (Ryan *et al.*, 1996).

As noted above, the maximum Cr content of garnets increases with *T*. However, the apparent *T* correlation arises from the linkage of temperature with depth in the Earth. The Cr content [and Cr/(Cr + Al)] of chromite coexisting with garnet increases with pressure, and this effect is relatively insensitive to temperature (Webb & Wood, 1986; Brey *et al.*, 1991). The partitioning of Cr between garnet and chromite is only mildly *T* sensitive, so that the Cr content of garnet that is in equilibrium with chromite (and hence Cr saturated) will rise with pressure; this is the basis of a technique for estimation

of geothermal gradients from garnet concentrates (Ryan *et al.*, 1996). The maximum Cr content observed at any temperature is lower in Tecton suites than in Archon suites (Fig. 3). This is consistent with a more elevated average geotherm in the younger mantle terranes. The maximum Cr contents of Proton suites at each T lie somewhat below those of Archon suites (Fig. 3), suggesting that Proton lithospheric mantle has geotherms higher, on average, than Archon lithospheric mantle.

The Cr content of garnet is most pressure sensitive when the garnet coexists with chromite, and the chromite + garnet assemblage is stable only in a limited range of bulk compositions at relatively low T (Webb & Wood, 1986). In Archon suites, chromite + garnet becomes unstable in most bulk compositions at depths corresponding to ~1000–1100°C; in Proton suites the higher average geotherm allows chromite + garnet to persist to higher T. In Tecton suites this assemblage potentially is stable to even higher T, but the requisite depleted bulk compositions appear to be rare (see below). In less refractory bulk compositions, or at temperatures greater than the limit of chromite + garnet stability, the Cr content of garnets is controlled only by bulk composition and partitioning with pyroxenes (Brey *et al.*, 1991). Smith & Boyd (1987) have shown that relatively small variations in X_{Cr} of garnet will be produced by P/T-induced changes in the garnet/pyroxene ratio, in a fixed bulk composition.

Depletion effects

In mantle-derived xenoliths, the Cr content of garnet is well correlated with generally accepted measures of depletion in 'basaltic' components (Fig. 9; Griffin *et al.*, 1998). High-Cr garnets are found in refractory rocks with high *mg*-number, low Ca and Al, low modal (cpx + gnt) and low cpx/gnt ratios, whereas low-Cr garnets are found in rocks that are more fertile by all of these measures. We therefore can use associations of other elements with Cr to evaluate the extent to which their concentrations are controlled by melt-extraction processes.

Fe and Cr show a strong negative correlation at all temperatures (Fig. 4); this is much stronger than the Mg–Cr association, which is influenced by the Ca–Cr relationship discussed above, and overrides the expected decrease of Fe content with temperature. This pattern is consistent with a major bulk-composition control on Fe content, through melt removal, at least in the shallower (lower-T) parts of the lithospheric mantle. At higher T, this process may be partly reversed by metasomatism (see below).

Y also shows a strong negative correlation with Cr content in the Archon and Proton suites, implying that Y has behaved as an incompatible element during the processes that have produced depletion in mantle peridotites. Because Y generally is regarded as being compatible in garnet, this behaviour may indicate that much of the garnet in many mantle peridotites was not present as a residual phase during the melting process, but has exsolved later from high-T pyroxenes, as suggested for Archon xenoliths by Cox *et al.* (1987). At low to intermediate temperatures Y shows a positive correlation with Fe, Ti, Ga and Zr, suggesting that all of these elements also have been removed as part of the depletion process (Fig. 6). However, Ti, Zr and Ga are not strongly negatively correlated with Cr at low temperature; this may partly reflect the relatively low precision for EMP measurements of Ti and PMP measurements of Ga at these levels. Low-T metasomatism may also disturb the Zr–Y relationship (see below) enough to obscure a Zr–Cr correlation.

These data, combined with observations on garnet composition as a function of rock composition (Fig. 9), suggest that Cr and Y in garnets are useful indicators of the degree of depletion in the host rock from which individual garnet grains were derived.

Metasomatic effects

Previous work (Griffin *et al.*, 1989*b*, 1999*a*; Smith *et al.*, 1991; Griffin & Ryan, 1995) has identified two prominent styles of metasomatism in peridotite xenoliths from Archean terranes. High-T (>1100°C) melt-related metasomatism, seen in sheared peridotite xenoliths from many kimberlites, involves the simultaneous introduction of Fe, Zr, Ti, Y and Ga (as well as Na, P and REE; Smith & Boyd, 1987), whereas low-T (900–1000°C) metasomatism commonly leads to preferential introduction of Zr relative to Y and Ti (Shee *et al.*, 1993; Griffin *et al.*, 1999*a*). The lower temperature range corresponds to the observed high values of Zr/Y centred on 1000°C, especially in Archon garnets (Fig. 3).

The high-T metasomatic process commonly produces garnets zoned to rims with lower Cr, lower *mg*-number and higher Fe than the cores. The correlations in the high-T garnets mirror those in these zoned garnets. The detailed shapes of the zoning profiles indicate significant growth of garnet (~50% of the observed garnet content) from introduced material during this process (Griffin *et al.*, 1989*b*, 1996*b*; Smith *et al.*, 1993), which in turn implies introduction of Al. The introduction of Fe is reflected in the good high-T correlations between FeO, TiO_2, Y and Zr (Figs 6 and 7), and in the flattening of the trends of FeO, MgO and *mg*-number vs T_{Ni} (Figs 2, 3 and 8). The high-T metasomatic introduction of Ti, Ga and Y also is apparent from the increasingly strong correlations among these elements at $T > 1000$°C (Figs 2, 3 and 6).

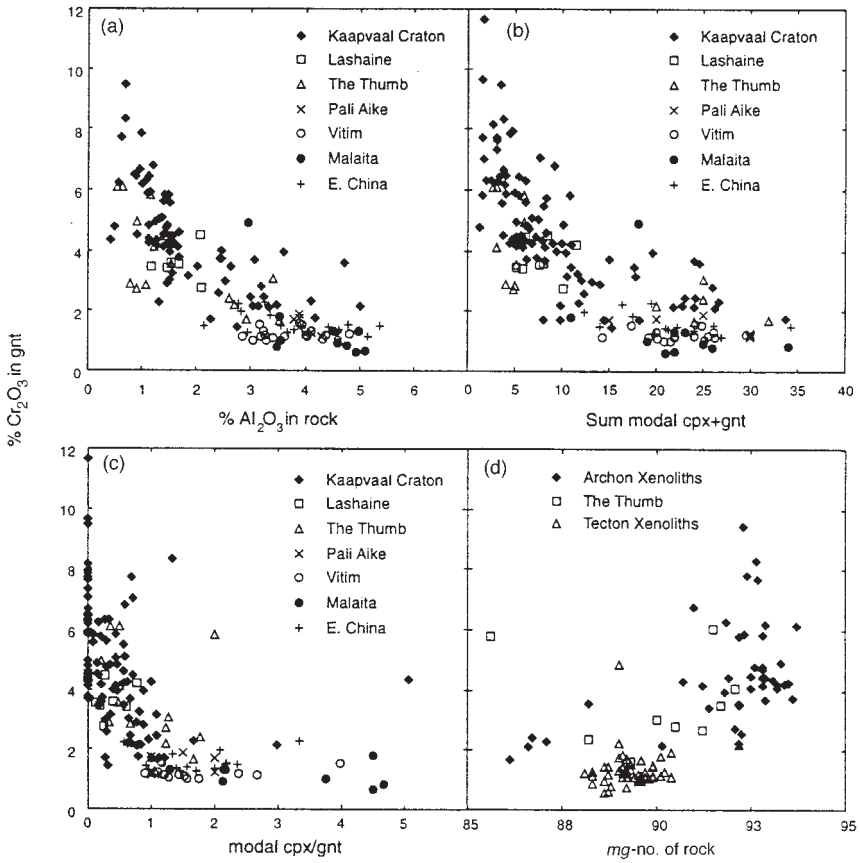

Fig. 9. Correlations between Cr_2O_3 content of garnet and composition of the host rock (after Griffin *et al.*, 1998). Low-Cr garnets are derived from relatively undepleted rocks rich in Ca, Al and Fe, whereas high-Cr garnets are derived from rocks depleted in these elements, with low (cpx + gnt) contents, low cpx/gnt, and high *mg*-number.

This high-T metasomatic process has been interpreted as the result of the infiltration of asthenospheric melts, especially along the foliation planes of deformed peridotites (Smith & Boyd, 1987; Smith *et al.*, 1991, 1993). Zoned garnets with such depleted cores and with overgrowth rims enriched in Y, Ti, Ga and Zr occur in many of the high-T deformed peridotite xenoliths from kimberlites, and the overgrowth rims are compositionally similar to many megacryst or 'discrete nodule' garnets in kimberlites and basalts, which may have crystallized from similar asthenosphere-derived melts (Griffin *et al.*, 1989*b*, 1996*b*; Smith *et al.*, 1991, 1993). The slopes of the mutual correlations between Y, Ti, Ga and Zr at high T, and the negative correlations of these elements with Cr, may be controlled by mixing between the depleted primary garnet compositions and the introduced material. The variations in these slopes between Archon, Proton and Tecton suites (Fig. 7) may reflect (1) differences in the mean composition of the depleted material (see below); (2) differences in the composition of melts at the lithosphere–asthenosphere boundary in different tectonic situations, and/or (3) pressure-dependent differences in melt–garnet partitioning related to the depth of the lithosphere–asthenosphere boundary in different tectonic settings.

If the pronounced break in slope of the Fe–T_{Ni} trends in Figs 2 and 3, and the similar variation in *mg*-number vs T in Fig. 8, are ascribed to the effect of metasomatism by asthenospheric melts, then the temperature of the break in slope (~1000–1100°C) may be a rough measure of the level to which such metasomatism typically reaches in different tectonic settings. The difference in geotherm from Archon to Proton to Tecton, implied by the different envelopes of Cr_{max} vs T_{Ni} (Fig. 3), requires that this temperature is reached at relatively shallow depths (~60–80 km) beneath Tectons, and greater depths (150–250 km) beneath Archons and Protons.

The Sr contents of pyrope garnets generally are low. However, significant contents (>3 ppm) are found in many Archon garnet suites, and to a lesser extent in Proton suites. Sr enrichment is most common in otherwise depleted garnets, and especially in harzburgitic types, so

that Sr tends to be positively associated with Cr and negatively associated with Y and Fe. Limited data from ion microprobe, laser-ablation inductively coupled plasma mass spectrometry (ICPMS) and isotope-dilution mass spectrometry show that Sr enrichment commonly is coupled with enrichment in light REE (LREE) and depletion in heavy REE (HREE), giving a sinuous REE pattern (Richardson *et al.*, 1984; Shimizu & Richardson, 1987; Hoal *et al.*, 1995; Griffin *et al.*, 1999*a*). This Sr–LREE enrichment has been interpreted as the result of carbonatite-related metasomatism acting upon already depleted rocks (Shimizu & Richardson, 1987; Griffin *et al.*, 1992), and may be genetically related to the formation of diamonds.

Lithospheric mantle stratigraphy and composition

The plots of element concentration against T for Archon suites (Fig. 3) illustrate several features common to Archean cratonic roots world-wide. The abundance of subcalcic harzburgite garnets in Archean mantle, relative to that beneath younger terranes, is illustrated in Fig. 5. The distribution of these garnets with depth is shown by plots of CaO, MgO and FeO vs T (Figs 3 and 7a), where they cluster strongly between 900 and 1100°C, corresponding to depths of ~140–180 km on typical cratonic geotherms. At shallower depths, these sections are dominated by moderately depleted lherzolites, with low average Ti, Y and Zr contents. At greater depths the dominant peridotitic rock type is a less depleted lherzolite, with higher concentrations of Ti, Zr, Y and Fe. The relative abundance of harzburgite and the degree of its stratigraphic concentration differ from craton to craton [see examples given by Griffin *et al.* (1996*a*, 1998)], but this basic pattern is common to most Archon mantle sections.

Proton mantle sections, in contrast, contain few low-Ca garnets, and these are nearly all low-Cr types, rather than the high-Cr subcalcic garnets common in Archon sections. They also tend to be concentrated at shallower depth; the main T range is 700–900°C, and on the higher average geotherms of Proton sections, this corresponds to depths of 100–120 km. Tecton sections seldom contain even mildly subcalcic garnets.

The median Cr content of the garnets decreases, and the mean Y content increases, from Archon to Proton to Tecton. This trend was noted by Griffin *et al.* (1998) on the basis of a smaller sample set, and correlated with a secular decrease in the degree of depletion of the subcontinental lithospheric mantle through the Earth's history. The accompanying steep rise in Y/Ga and decrease in Zr/Y from Archon to Tecton suites was modelled (Griffin *et al.*, 1998) as reflecting a corresponding rise in mantle fertility, expressed as modal (cpx + gnt) and cpx/gnt, in newly created lithospheric mantle from Archean time to the present (see Fig. 9).

There is no significant difference in *mg*-number between Proton and Tecton garnets in this dataset. The median *mg*-number of Archon garnets is slightly higher than that of Proton or Tecton garnets, and this could reflect both the abundance of garnets from depleted harzburgitic compositions and a higher degree of depletion in the rocks from which lherzolitic garnets are derived. These more depleted rocks would be expected to have more magnesian olivine, and hence more magnesian garnet at any T.

In all three settings, the flattening of the Fe–T_{Ni} curve with depth suggests a variation of olivine composition with depth. Figure 8 shows the trend of garnet *mg*-number vs T expected from Fe–Mg partitioning with olivine of fixed compositions. The trend observed in the complete dataset is generally flatter than predicted, and the degree of divergence increases with temperature. This suggests that on a world-wide scale, the composition of mantle olivine becomes more iron rich toward the base of the lithosphere. This trend may reflect both progressively greater degrees of melt extraction toward the top of the lithosphere and greater degrees of interaction with asthenosphere-derived melts, as shown by the corresponding increases in the mean concentrations of elements such as Y, Zr, Ti and Ga documented here (Figs 3 and 7; Gaul *et al.*, in preparation).

Garnet populations

The scatter plots, and particularly the chi-plots of Figs 4 and 6, show complex but resolvable relationships between many element pairs. This complexity remains even when the data are broken down into temperature intervals (Fig. 6) or by tectonic setting (not shown), and many interelement correlations vary differently with temperature in different tectonic settings, as discussed above. These variations suggest that it is possible to define statistically meaningful populations of garnet on the basis of major- and trace-element composition, and to map the vertical and lateral distribution of these in the lithospheric mantle. Methods for defining these populations, and their distribution in selected mantle sections, will be the subject of a separate paper.

CONCLUSIONS

(1) Mn and Zn contents of Cr-pyrope garnets show similar temperature dependence world-wide, and probably are controlled by T-dependent partitioning between garnet and mantle olivine, as is the case for Ni. The expected

correlation of Fe/Mg with T is largely masked by effects of crystal chemistry and bulk composition.

(2) The Cr content of garnet is a primary indicator of the degree of depletion of the host rock; Fe, Y, Ti and Ga show strong negative correlations with Cr, suggesting that all have been removed as part of the primary depletion process.

(3) High-temperature metasomatism, reflecting the introduction of asthenospheric melts and the consequent growth of new garnet, is widespread in the deeper parts of lithosphere of all ages. It produces strong positive correlations between Fe, Zr, Ti, Y and Ga, and leads to 'refertilization' of previously depleted rocks. The mean Fo content of mantle olivine decreases with depth in Archean and Proterozoic lithosphere, and this may reflect both an upward increase in primary depletion, and metasomatism by asthenosphere-derived fluids near the base of the lithosphere.

(4) The prominent Ca–Cr correlation (the 'lherzolite trend') seen in garnets from clinopyroxene-bearing ultramafic rocks is controlled primarily by the Cr/Al content of the host rock. High Cr contents in Ca-saturated garnets require high Ca contents, and Ca is negatively correlated with Mg. The position and slope of the lherzolite trend vary with temperature and tectonic setting, suggesting that P/T ratio exerts a control on Ca/Cr.

(5) Garnets with less Ca than the lherzolite trend ('subcalcic garnets') are largely confined to Archon suites, where they show a strong concentration in the 140–180 km depth range (T = 900–1100°C). The rare subcalcic garnets from Proton suites typically are low-Cr types and occur at shallower depths (100–120 km; T = 700–1000°C). Subcalcic garnets are absent in Tecton suites analysed here.

(6) Variations in Cr and Y contents, and in Y/Ga and Zr/Y ratios, of garnets with T_{Ni} < 1200°C largely reflect primary depletion, and these data show that the average degree of depletion in the lithospheric mantle decreases from Archon to Proton to Tecton.

(7) This analysis illustrates the usefulness of effective graphical analysis for elucidating important features of the data and highlighting aspects worthy of further investigation. Apart from anything else, this sort of exploratory analysis is a necessary antecedent to the application of more sophisticated statistical analysis.

(8) The complexity of the geochemical relationships illustrated here, and their variation with temperature and tectonic setting, suggests that it is possible to define meaningful compositional populations of garnets, which can be used to map the stratigraphy and structure of the lithospheric mantle.

ACKNOWLEDGEMENTS

This is Contribution 139 from the ARC National Key Centre for Geochemical Evolution and Metallogeny of Continents (GEMOC). The work presented here has benefited from many discussions with Norm Pearson, as well as Buddy Doyle, Bram Janse, Simon Shee and Bruce Wyatt. Analytical work and the statistical analysis has been supported by grants from the Australian Research Council, the Australian Department of Industry, Science and Technology, and Macquarie University. The original version of the manuscript was improved by thoughtful and constructive reviews from Doug Smith and Gerhard Brey.

REFERENCES

Boyd, F. R. (1989). Composition and distinction between oceanic and cratonic lithosphere. *Earth and Planetary Science Letters* **96,** 15–26.

Boyd, F. R. (1997). Origin of peridotite xenoliths: major element considerations. In: Ranalli, G., Ricci Lucchi, F., Ricci, C. A. & Trommsdorff, T. (eds) *High Pressure and High Temperature Research on Lithosphere and Mantle Materials*. University of Sienna.

Boyd, F. R. & Mertzman, S. A. (1987). Composition and structure of the Kaapvaal lithosphere, southern Africa. In: Mysen, B. O. (ed.) *Magmatic Processes: Physicochemical Principles. Geochemical Society Special Publication* **1,** 13–24.

Boyd, F. R., Pearson, D. G., Nixon, P. H. & Mertzman, S. A. (1993). Low-calcium garnet harzburgites from southern Africa: their relations to craton structure and diamond crystallization. *Contributions to Mineralogy and Petrology* **113,** 352–366.

Boyd, F. R., Pokhilenko, N. P., Pearson, D. G., Mertzman, S. A., Sobolev, N. V. & Finger, L. W. (1997). Composition of the Siberian cratonic mantle: evidence from Udachnaya peridotite xenoliths. *Contributions to Mineralogy and Petrology* **128,** 228–246.

Brenker, F. E. & Brey, G. P. (1997). Reconstruction of the exhumation path of the Alpe Arami garnet-peridotite body from depths exceeding 160 km. *Journal of Metamorphic Geology* **15,** 581–592.

Brey, G. P. (1989). Geothermobarometry for lherzolites: experiments from 10 to 60 kb, new thermobarometers and application to natural rocks. Habilitations Thesis, Technische Hochschule Darmstadt, Germany.

Brey, G. P., Doroshev, A. & Kogarko, L. (1991). The join pyrope–knorringite: experimental constraints for a new geothermobarometer for coexisting garnet and spinel. *Extended Abstracts, 5th International Kimberlite Conference*. Novosibirsk: pp. 26–28.

Brown, R. W., Gallagher, K., Griffin, W. L., Ryan, C. G., de Wit, M. C. J., Belton, D. X. & Harman, R. (1998). Kimberlites, accelerated erosion and evolution of the lithospheric mantle beneath the Kaapvaal craton during the mid-Cretaceous. *Extended Abstracts, 7th International Kimberlite Conference*. Cape Town: pp. 105–107.

Canil, D. (1994). An experimental calibration of the 'Nickel in Garnet' geothermometer with applications. *Contributions to Mineralogy and Petrology* **117,** 410–420.

Cox, K. G., Smith, M. R. & Beswetherick, S. (1987). Textural studies of garnet lherzolites: evidence of exsolution origin from high-temperature harzburgites. In: Nixon, P. H. (ed.) *Mantle Xenoliths*. New York: John Wiley, pp. 537–550.

Fisher, N. I. & Switzer, P. (1985). Chi-plots for assessing dependence. *Biometrika* **72,** 253–265.

Griffin, W. L. & Ryan, C. G. (1995). Trace elements in indicator minerals: area selection and target evaluation in diamond exploration. *Journal of Geochemical Exploration* **53,** 311–337.

Griffin, W. L. & Ryan, C. G. (1996). 'An experimental calibration of the 'Nickel in Garnet' geothermometer, with applications' by D. Canil: discussion. *Contributions to Mineralogy and Petrology* **124,** 216–218.

Griffin, W. L., Ryan, C. G., Cousens, D. C., Sie, S. H. & Suter, G. F. (1989*a*). Ni in Cr-pyrope garnets: a new geothermometer. *Contributions to Mineralogy and Petrology* **103,** 199–202.

Griffin, W. L., Smith, D., Boyd, F. R., Cousens, D. R., Ryan, C. G., Sie, S. H. & Suter, G. F. (1989*b*). Trace element zoning in garnets from sheared mantle xenoliths. *Geochimica et Cosmochimica Acta* **53,** 561–567.

Griffin, W. L., Gurney, J. J. & Ryan, C. G. (1992). Variations in trapping temperatures and trace elements in peridotite-suite inclusions from African diamonds: evidence for two inclusion suites, and implications for lithosphere stratigraphy. *Contributions to Mineralogy and Petrology* **110,** 1–15.

Griffin, W. L., Kaminsky, F. V., O'Reilly, S. Y., Ryan, C. G. & Sobolev, N. V. (1995). Mapping the Siberian lithosphere with garnets and spinels. *Extended Abstracts, 6th International Kimberlite Conference*. Novosbirsk: pp. 194–195.

Griffin, W. L., Kaminsky, F. V., Ryan, C. G., O'Reilly, S. Y., Win, T. T. & Ilupin, I. P. (1996*a*). Thermal state and composition of the lithospheric mantle beneath the Daldyn kimberlite field, Yakutia. *Tectonophysics* **262,** 19–33.

Griffin, W. L., Smith, D., Ryan, C. G., O'Reilly, S. Y. & Win, T. T. (1996*b*). Trace element zoning in mantle minerals: metasomatism and thermal events in the upper mantle. *Canadian Mineralogist* **34,** 1179–1193.

Griffin, W. L., O'Reilly, S. Y., Ryan, C. G., Gaul, O. & Ionov, D. I. (1998). Secular variation in the composition of subcontinental lithospheric mantle: geophysical and geodynamic implications. In: Braun, J., Dooley, J. C., Goleby, B. R., van der Hilst, R. D. & Klootwijk, C. T. (eds) *Structure and Evolution of the Australian Continent, Geodynamics Volume 26*. Washington, DC: American Geophysical Union, pp. 1–26.

Griffin, W. L., Ryan, C. G., Kaminsky, F. V., O'Reilly, S. Y., Natapov, L. M., Win, T. T., Kinny, P. D. & Ilupin, I. P. (1999*a*). The Siberian lithosphere traverse: mantle terranes and the assembly of the Siberian Craton. *Tectonophysics* (in press).

Griffin, W. L., Shee, S. H., Ryan, C. G., Win, T. T. & Wyatt, B. A. (1999*b*). Harzburgite to lherzolite and back again: metasomatic processes in ultramafic xenoliths from the Wesselton kimberlite, Kimberley, South Africa. *Contributions to Mineralogy and Petrology* (in press).

Gurney, J. J. (1984). A correlation between garnets and diamonds. In: Glover, J. E. & Harris, P. G. (eds) *Kimberlite Occurrence and Origins: a Basis for Conceptual Models in Exploration. Geology Department and University Extension, University of Western Australia, Publication* **8,** 143–166.

Gurney, J. J. & Zweistra, P. (1995). The interpretation of the major element compositions of mantle minerals in diamond exploration. *Journal of Geochemical Exploration* **53,** 293–310.

Hoal, B. G., Hoal, K. E. O., Boyd, F. R. & Pearson, D. G. (1995). Age constraints on crustal and mantle lithosphere beneath the Gibeon kimberlite field, Namibia. *Suid-Afrikaanse Tydskrif Geol.* **98,** 112–118.

Janse, A. J. A. (1994). Is Clifford's Rule still valid? Affirmative examples from around the world. In: Meyer, H. O. A. & Leonardos, O. (eds) *Diamonds: Characterisation, Genesis and Exploration. CPRM Special Publication 1A/93*. Brasilia: Pesquisa de Recursos Minerais, pp. 215–235.

Kopylova, M. G., Russel, J. K. & Cookenboo, H. (1999). Petrology of peridotite and pyroxenite xenoliths from the Jericho kimberlite: implications for the thermal state of the mantle beneath the Slave craton, northern Canada. *Journal of Petrology* **40,** 79–104.

Morgan, P. (1995). Diamond exploration from the bottom up. *Journal of Geochemical Exploration* **53,** 145–166.

Nickel, K. G. (1983). Petrogenesis of garnet and spinel peridotites. Ph.D. Thesis, University of Tasmania, Hobart, Australia.

Nixon, P. H. (1987). Kimberlitic xenoliths and their cratonic setting. In: Nixon, P. H. (ed.) *Mantle Xenoliths*. New York: John Wiley, pp. 215–239.

O'Neill, H. St C. & Wood, B. J. (1979). An experimental study of Fe–Mg partitioning between garnet and olivine and its calibration as a geothermometer. *Contributions to Mineralogy and Petrology* **70,** 59–70.

O'Reilly, S. Y. & Griffin, W. L. (1985). A xenolith-derived geotherm for southeastern Australia and its geophysical implications. *Tectonophysics* **111,** 41–63.

O'Reilly, S. Y. & Griffin, W. L. (1995). Trace element partitioning between garnet and clinopyroxene in mantle-derived pyroxenites and eclogites: *P–T–X* controls. *Chemical Geology* **121,** 105–130.

O'Reilly, S. Y. & Griffin, W. L. (1996). 4-D lithospheric mapping: a review of the methodology with examples. *Tectonophysics* **262,** 3–18.

O'Reilly, S. Y., Chen, D., Griffin, W. L. & Ryan, C. G. (1997). Minor elements in olivine from spinel peridotite xenoliths: implications for thermobarometry. *Mineralogical Magazine* **61,** 257–269.

Richardson, S. H., Gurney, J. J., Erlank, A. J. & Harris, J. W. (1984). Origin of diamonds in old enriched lithosphere. *Nature* **310,** 198–202.

Ryan, C. G., Cousens, D. R., Sie, S. H., Griffin, W. L. & Clayton, E. J. (1990). Quantitative PIXE microanalysis in the geosciences. *Nuclear Instruments and Methods* **B47,** 55–71.

Ryan, C. G., Griffin, W. L. & Pearson, N. J. (1996). Garnet geotherms: a technique for derivation of *P–T* data from Cr-pyrope garnets. *Journal of Geophysical Research* **101,** 5611–5625.

Schulze, D. J. (1995). Low-Ca garnet harzburgites from Kimberley, South Africa: abundance and bearing on the structure and evolution of the lithosphere. *Journal of Geophysical Research* **100,** 12513–12526.

Shee, S. R., Wyatt, B. A. & Griffin, W. L. (1993). Major and trace element mineral chemistry of peridotite xenoliths from the Wesselton kimberlite, South Africa. *IAVCEI Abstracts, Canberra,* **93**.

Shimizu, N. & Richardson, S. H. (1987). Trace element abundance patterns of garnet inclusions in peridotite-suite diamonds. *Geochimica et Cosmochimica Acta* **51,** 755–758.

Smith, D. & Boyd, F. R. (1987). Compositional heterogeneities in a high-temperature lherzolite nodule and implications for mantle processes. In: Nixon, P. H. (ed.) *Mantle Xenoliths*. New York: John Wiley: pp. 551–562.

Smith, D., Griffin, W. L., Ryan, C. G., Cousens, D. R., Sie, S. H. & Suter, G. F. (1991). Trace-element zoning of garnets from The Thumb: a guide to mantle processes. *Contributions to Mineralogy and Petrology* **107,** 60–79.

Smith, D., Griffin, W. L. & Ryan, C. G. (1993). Compositional evolution of high-temperature sheared lherzolite PHN1611. *Geochimica et Cosmochimica Acta* **57,** 605–613.

Smyth, J. R. & Bish, D. L. (1988). *Crystal Structures and Cation Sites of the Rock-forming Minerals*. Sydney: Allen and Unwin, 332 pp.

Smyth, J. R. & McCormick, T. C. (1995). Crystallographic data for minerals. In: Ahrens, T. J. (ed.) *Mineral Physics and Crystallography: a Handbook of Physical Constants*. Washington, DC: American Geophysical Union, pp. 1–17.

Sobolev, N. V., Lavrent'ev, Yu. G., Pokhilenko, N. P. & Usova, L. V. (1973). Chrome-rich garnets from the kimberlites of Yakutia and their parageneses. *Contributions to Mineralogy and Petrology* **40,** 39–52.

Spetsius, Z. V. (1995). Occurrence of diamond in the mantle: a case study from the Siberian Platform. *Journal of Geochemical Exploration* **53,** 25–40.

Webb, S. A. C. & Wood, B. J. (1986). Spinel–pyroxene–garnet relationships and their dependence on Cr/Al ratio. *Contributions to Mineralogy and Petrology* **92,** 471–480.

Wood, B. J. & Holloway, J. R. (1984). A thermodynamic model for subsolidus equilibria in the system CaO–MgO–Al_2O_3–SiO_2. *Geochimica et Cosmochimica Acta* **48,** 159–176.

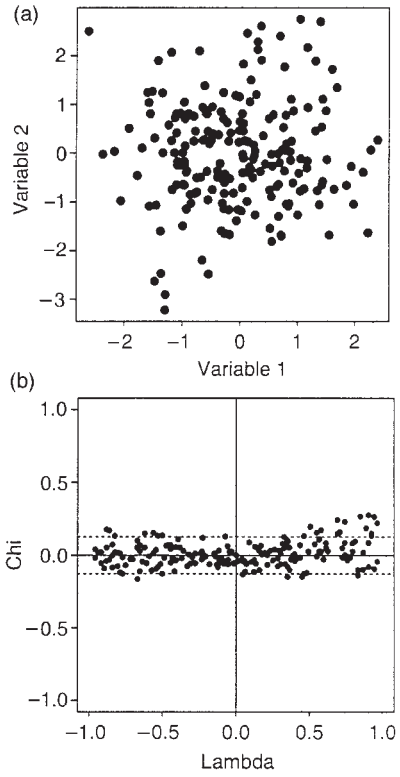

Fig. A1. Scatterplot and chi-plot of two unrelated variables.

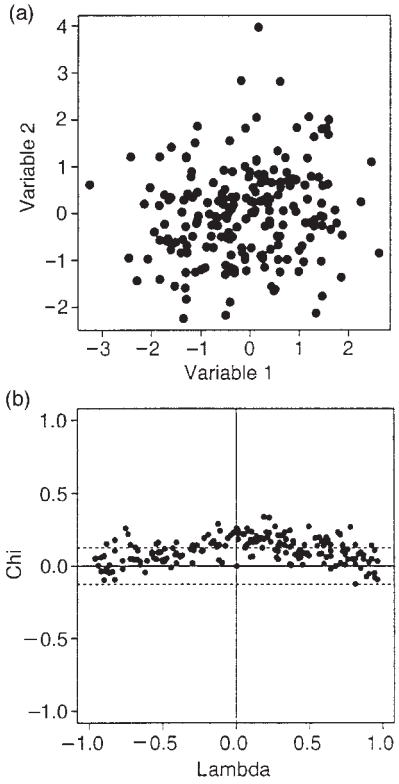

Fig. A2. Scatterplot and chi-plot of two variables with a weak positive association.

APPENDIX A

The chi-plot: a graphical method for assessing the relationship between two variables

The usual graphical method of assessing the relationship between two variables is a scatterplot. However, when a large amount of data is available, or when there is a moderately subtle relationship between the variables, the large number of points being plotted can make an interesting pattern difficult to detect. The chi-plot (or χ-plot) is used to supplement a scatterplot, by producing characteristic patterns of points for different types of relationships, and even when there is *no* relationship between the variables. The following pairs of plots (scatterplot plus chi-plot) indicate how it works. A brief algorithm for producing a chi-plot is given at the end.

The scatterplots of the variables have been plotted on a log scale for ease of visualization.

No association

Figure A1(a) is a scatterplot of 200 measurements on two unrelated variables. The corresponding chi-plot is shown in Fig. A1(b); the plotted values tend to lie within the 95% control lines, with approximately $2\frac{1}{2}$% above the upper control line and $2\frac{1}{2}$% below the lower control line.

Weak association

Figure A2(a) is a scatterplot of 200 measurements on two variables that have a weak positive relationship: that is, there is a small tendency for large [small] values of one variable to correspond to large [small] values of the other. The corresponding chi-plot is shown in Fig. A2(b). Now the pattern of plotted values has a small but perceptible tent-like shape, and points have moved somewhat upwards on the graph. Rather more than $2\frac{1}{2}$% are plotting above the upper control line, and less than $2\frac{1}{2}$% below the lower control line.

In contrast, weak negative association would appear as in Fig. A3(a) and (b).

Strong association

Figure A4(a) is a scatterplot of 200 measurements on two variables that have a strong positive relationship. This is clearly evident in the scatterplot, so the corresponding chi-plot is shown in Fig. A4(b) for interest only. As we move towards the extreme, where one variable is very

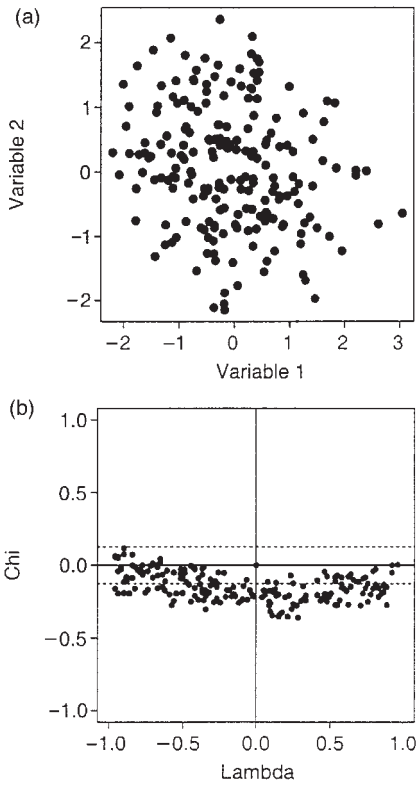

Fig. A3. Scatterplot and chi-plot of two variables with a weak negative association.

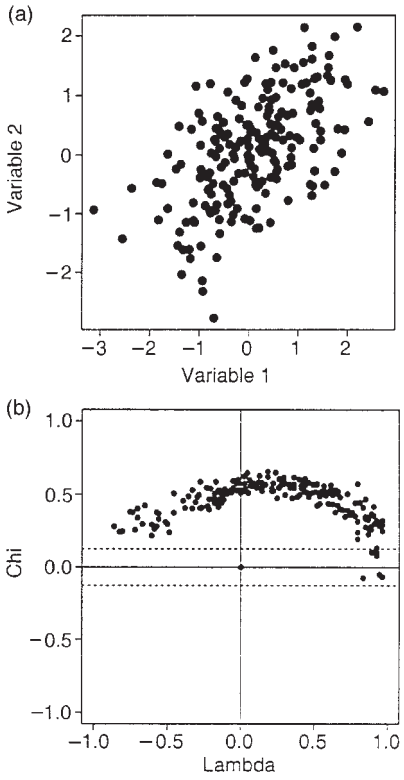

Fig. A4. Scatterplot and chi-plot of two variables with a strong positive association.

strongly correlated with the other, the plot appears as in Fig. A5.

Unusual association

Sometimes, there may be no obvious association in a scatterplot, and the sample correlation coefficient may be very close to zero, yet there may be a relationship between the variables that it is important to detect. Such relationships can be detected by a chi-plot. One manifestation of this would be a chi-plot with points still centred around the axis $\chi = 0$, but with many plotting outside the control limits [see (i) below]. Another might be a chi-plot with the points for $\lambda < 0$ splitting into two groups [see (ii) below]. Physical mechanisms leading to such aberrant behaviour in chi-plots could be the following:

(i) data below a detection limit are recorded as being at the detection limit;

(ii) measurements from different populations are inadvertently mixed.

An example is given in Fig. A6. In this case, there is a mixture of two populations. In the first population, each variable tends to have lower values, and the variables are negatively associated; whereas in the second, the variables tend to have higher values and tend to be positively associated. As can be seen in Fig. A6(b), the points corresponding to $\lambda < 0$ are grouped into two 'lobes'. Examples of this sort of behaviour are not uncommon in practice.

Algorithm for graphing chi-plot variables

Let $(x_1, y_1), \ldots, (x_n, y_n)$, be n pairs of measurements on two variables X and Y. Let $I(A)$ be a function of an event A such that $I(A) = 1$ if A is true, and $I(A) = 0$ otherwise. For each data point (x_i, y_i), we calculate

$$H_i = \sum_{j \neq i} I(x_j \leq x_i, y_j \leq y_i)/(n-1)$$

$$F_i = \sum_{j \neq i} I(x_j \leq x_i)/(n-1)$$

$$G_i = \sum_{j \neq i} I(y_j \leq y_i)/(n-1)$$

$$S_i = \text{sign}\{(F_i - \tfrac{1}{2})(G_i - \tfrac{1}{2})\}.$$

Now we calculate

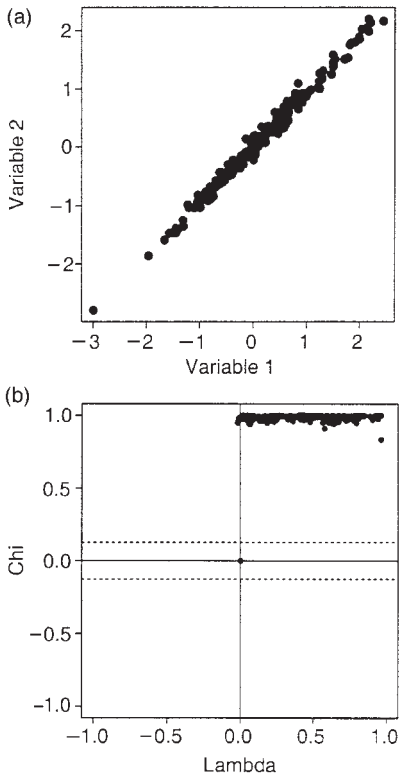

Fig. A5. Scatterplot and chi-plot of two variables with a very strong positive association.

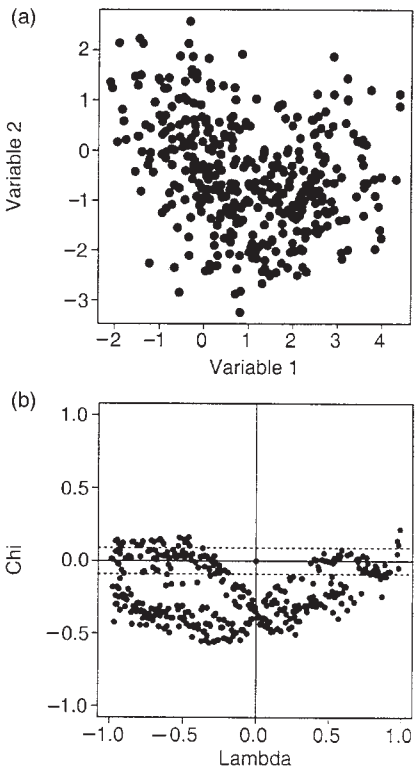

Fig. A6. Scatterplot and chi-plot of a sample consisting of a mixture of two populations with different associations between the variables.

$$\chi_i = (H_i - F_i G_i)/\{F_i(1-F_i)G_i(1-G_i)\}^{1/2}$$

and

$$\lambda_i = 4S_i \max\{(F_i - \tfrac{1}{2})^2, (G_i - \tfrac{1}{2})^2\}.$$

A χ-plot is a scatterplot plot of the pairs (λ_i, χ_i) for which

$$|\lambda_i| < 4\left\{\frac{1}{n-1} - \frac{1}{2}\right\}^2.$$

It is helpful to insert horizontal 'control' lines for the χ values at pre-specified significance levels. The levels recommended in the original reference have been re-computed more precisely, for 90%, 95% and 99% levels. If there is no relationship between X and Y, most of the points should plot between these two lines.

It is useful to be able to interpret the λ values. λ_i is related to the distance of the point x_i, y_i from the 'centre' of the datasets as measured by $(\tilde{x}, \tilde{y})$, where $\tilde{x}$ is the median (middle) value amongst $x_1, \ldots, x_n$ and similarly for $\tilde{y}$. A positive value of λ_i means that both x_i and y_i are large relative to their respective medians, or both small; whereas a negative value of λ_i corresponds to x_i and y_i being on opposite sides of their respective medians.

Appendix B: Locality data

Locality	Continent/region	Rock*	Tectonic unit†	No. anal.	Locality	Continent/region	Rock*	Tectonic unit†	No. anal.
Archons					*Protons*				
101k2	Africa	K	Tanzanian C	5	Deutsche Erde	Africa	K	Namaqua FB	54
64K1	Africa	K	Tanzanian C	7	Gruen Dorner	Africa	K	Namaqua FB	10
67K2	Africa	K	Tanzanian C	8	Rietfontein	Africa	K	Kalahari C	42
80K6	Africa	K	Tanzanian C	44	Sekameng	Africa	K	Kalahari C	75
99K2	Africa	K	Tanzanian C	52	Uintjiesberg	Africa	K	Kalahari C	36
Bakwanga	Africa	K	Central Africa C	16	Baltiiskaya	Siberia	K	Siberian C	15
Cirque	Africa	K	W. Africa C	10	Bezymyannaya	Siberia	K	Siberian C	6
Colossus	Africa	K	Kalahari C	34	Chomur	Siberia	K	Siberian C	51
Dokolwayo	Africa	K	Kalahari C	48	Dama	Siberia	K	Siberian C	43
Dutoitspan	Africa	K	Kalahari C	6	Dianga	Siberia	K	Siberian C	7
Finsch	Africa	K	Kalahari C	65	Druzhba	Siberia	K	Siberian C	37
Frank Smith	Africa	K	Kalahari C	50	Granatovaya	Siberia	K	Siberian C	21
S. Renecke	Africa	A	Kalahari C	400	Khrizolitovaya	Siberia	K	Siberian C	66
Gope 25	Africa	K	Kalahari C	37	Krasivaya	Siberia	K	Siberian C	7
Jwaneng	Africa	K	Kalahari C	52	Kuranakhskaya	Siberia	K	Siberian C	8
Kamfersdam	Africa	K	Kalahari C	54	Lykhchan	Siberia	K	Siberian C	10
Kao	Africa	K	Kalahari C	50	Makarovskaya	Siberia	K	Siberian C	105
Klipfontein	Africa	K	Kalahari C	43	Meri	Siberia	K	Siberian C	8
Koffiefontein	Africa	K	Kalahari C	42	Muza	Siberia	K	Siberian C	125
Lace	Africa	K	Kalahari C	68	Nadyozhnaya	Siberia	K	Siberian C	77
Leicester	Africa	K	Kalahari C	27	Nemagnitnaya	Siberia	K	Siberian C	60
Letlhakane	Africa	K	Kalahari C	23	Nevlovivaya	Siberia	K	Siberian C	24
Letseng	Africa	K	Kalahari C	30	Obnazhennaya	Siberia	K	Siberian C	128
Liqhobong	Africa	K	Kalahari C	35	Olimp	Siberia	K	Siberian C	20
Luanza	Africa	K	Central Africa C	31	Operatorskaya	Siberia	K	Siberian C	14
Makibulei	Africa	K	Tanzanian C	47	Universitetskaya	Siberia	K	Siberian C	87
Mali 117	Africa	K	W. Africa C	115	Vtorogodnitsa	Siberia	K	Siberian C	44
Mwadui	Africa	K	Tanzanian C	94	Yegorich	Siberia	K	Siberian C	24
National	Africa	K	Kalahari C	18	Umbinskaya A	E. Russia	K	Timan	75
Newlands	Africa	K	Kalahari C	74	Umbinskaya C	E. Russia	K	Timan	28
Orapa	Africa	K	Kalahari C	75	Aultman 1	N. America	K	Laurentian O	58

Locality	Continent/region	Rock*	Tectonic unit†	No. anal.	Locality	Continent/region	Rock*	Tectonic unit†	No. anal.
Premier	Africa	K	Kalahari C	6	Bacon's Pipe	N. America	K	Superior Province	27
Quest 1	Africa	K	Kalahari C	31	Buell Park	N. America	K	Laurentian O	81
Quest 2	Africa	K	Kalahari C	35	Chicken Park	N. America	K	Laurentian O	50
Quest 3	Africa	K	Kalahari C	37	Crystal	N. America	K	Superior Province	60
River Ranch	Africa	K	Kalahari C	86	Garnet Ridge	N. America	K	Laurentian O	134
Roberts Victor	Africa	K	Kalahari C	175	George Creek	N. America	K	Laurentian O	63
Snyder	Africa	A	Kalahari C	14	Green Knobs	N. America	K	Laurentian O	43
Sover	Africa	K	Kalahari C	13	Iron Mountain	N. America	K	Laurentian O	37
SPL14	Africa	K	Kalahari C	56	Kelsey Lake 1	N. America	K	Laurentian O	81
Star	Africa	K	Kalahari C	38	Kelsey Lake 2	N. America	K	Laurentian O	56
Sultan	Africa	K	Tanzanian C	25	Lake Ellen	N. America	K	Superior Province	59
Wesselton	Africa	K	Kalahari C	193	Michigan	N. America	K	Superior Province	385
Zero	Africa	K	Kalahari C	28	Moses Rock	N. America	K	Laurentian O	41
Aerogeology	Siberia	K	Siberian C	31	Prairie Creek	N. America	L	Laurentian O	65
Aikhal	Siberia	K	Siberian C	79	Sloan 1	N. America	K	Laurentian O	57
Amakinskaya	Siberia	K	Siberian C	131	Sloan 2	N. America	K	Laurentian O	73
Dalnaya	Siberia	K	Siberian C	107	Sloan 5	N. America	K	Laurentian O	52
Geophysichiskaya	Siberia	K	Siberian C	102	Twin Knobs	N. America	L	Laurentian O	43
Internationalnaya	Siberia	K	Siberian C	60	Williams	N. America	K	Wyoming C	58
Iskorka	Siberia	K	Siberian C	41	Wisconsin	N. America	A	Laurentian O	181
Kollektivnaya	Siberia	K	Siberian C	78	Batty	N. America	K	Rae Province	32
Komsomolonaya	Siberia	K	Siberian C	43	Fort a la Corne	N. America	K	Trans-Hudson O	81
Krasnopresnenskaya	Siberia	K	Siberian C	8	JBL 8	N. America	K	Hearne Province	28
Marshrutnaya	Siberia	K	Siberian C	44	JBL 10	N. America	K	Hearne Province	32
Mir	Siberia	K	Siberian C	135	Pipe U	N. America	K	Hearne Province	50
Molodost	Siberia	K	Siberian C	34	Rhonda	N. America	K	Trans-Hudson O	102
Motorchuna	Siberia	A	Siberian C	25	Sturgeon Lake	N. America	K	Trans-Hudson O	10
Nachalnaya	Siberia	K	Siberian C	110	Boa Esperanca	S. America	K	Brazil, Prot.	24
Nedelec	Siberia	K	Siberian C	42	Cana Verde	S. America	K	Brazil, Prot.	32
NIIGA	Siberia	K	Siberian C	150	El Candado	S. America	K	Guyana C	57
Novinka	Siberia	K	Siberian C	43	El Cordero	S. America	K	Guyana C	41
Osennaya	Siberia	K	Siberian C	45	El Cristo	S. America	K	Guyana C	10

Appendix B: continued

Locality	Continent/region	Rock*	Tectonic unit†	No. anal.	Locality	Continent/region	Rock*	Tectonic unit†	No. anal.
Petrogradskaya	Siberia	K	Siberian C	17	JBMT-05	S. America	K	Brazil, Prot.	21
Radiogeologicheskaya	Siberia	K	Siberian C	63	JBMT-09	S. America	K	Brazil, Prot.	20
Radiovolvonaya	Siberia	K	Siberian C	30	JBMT-17	S. America	K	Brazil, Prot.	19
Svetlaya	Siberia	K	Siberian C	98	La Ceniza	S. America	K	Guyana C	8
Sytykanskaya	Siberia	K	Siberian C	83	MPJU-T02	S. America	K	Brazil, Prot.	20
Tayozhnaya	Siberia	K	Siberian C	119	Hunan	China	A	Yangtze C	11
Udachnaya	Siberia	K	Siberian C	579	Jingshan 1	China	L	Yangtze C	17
Vostok	Siberia	K	Siberian C	36	Jingshan 7	China	L	Yangtze C	20
Yakutskaya	Siberia	K	Siberian C	51	Maping 1	China	L	Yangtze C	30
Yubileinaya	Siberia	K	Siberian C	75	Xiangchong	China	L	Yangtze C	5
Zapolarnaya	Siberia	K	Siberian C	124	AH1971	Australia	A	S. Australia C	36
Zarnitza	Siberia	K	Siberian C	139	AH1972	Australia	A	S. Australia C	15
Zimnaya	Siberia	K	Siberian C	107	Argyle	Australia	L	N. Australia C	17
Archangelskaya	E. Russia	K	Baltic Shield	50	Buljah	Australia	UML	W. Australia C	30
Anom. 734/5	E. Russia	K	Baltic Shield	115	Calcutteroo	Australia	K	S. Australia C	39
Anom. 734/8	E. Russia	K	Baltic Shield	105	Carnarvon	Australia	A	W. Australia C	81
Anom. 734/9	E. Russia	K	Baltic Shield	90	Century Creek	Australia	L	W. Australia C	42
Karpinskaya 1	E. Russia	K	Baltic Shield	35	Cleve	Australia	K	S. Australia C	41
Karpinskaya 2	E. Russia	K	Baltic Shield	39	El Alamein	Australia	K	S. Australia C	54
Lomonosova	E. Russia	K	Baltic Shield	88	Ellendale 4	Australia	L	N. Australia C	108
Pachuga	E. Russia	K	Baltic Shield	49	Ellendale 7	Australia	L	N. Australia C	32
Pioneerskaya	E. Russia	K	Baltic Shield	85	Ellendale 9	Australia	L	N. Australia C	33
Pomorskaya	E. Russia	K	Baltic Shield	24	Ellendale 13	Australia	L	N. Australia C	11
Lahtojoki	E. Russia	K	Baltic Shield	45	Eurelia K6	Australia	K	S. Australia C	38
Solokha	E. Russia	K	Baltic Shield	39	Eurelia K7	Australia	K	S. Australia C	47
A154	N. America	K	Slave C	55	Eurelia K13	Australia	K	S. Australia C	56
A21	N. America	K	Slave C	56	Jewill	Australia	UML	W. Australia C	49
APK1	N. America	K	Slave C	35	Melrose	Australia	UML	W. Australia C	76
APK2	N. America	K	Slave C	30	Mount Hope	Australia	K	S. Australia C	104
DO18	N. America	K	Slave C	25	Mungibbie	Australia	K	S. Australia C	48
DO27	N. America	K	Slave C	143	Pine Creek	Australia	K	S. Australia C	114
EGO3	N. America	K	Slave C	54	Springfield	Australia	A	S. Australia C	96

Locality	Continent/region	Rock*	Tectonic unit†	No. anal.	Locality	Continent/region	Rock*	Tectonic unit†	No. anal.
Humpy Lake	N. America	K	Slave C	30	Sugarloaf Dam	Australia	K	S. Australia C	121
Point Lake	N. America	K	Slave C	68	Wandagee	Australia	UML	W. Australia C	35
Ranch Lake	N. America	K	Slave C	101	Wonna Gorge	Australia	K	S. Australia C	9
Hongqi 1	China	K	Sino-Korean C	45	**Total**	**101**		**16**	**5013**
Hongxi 27	China	K	Sino-Korean C	24					
Liaoning 42	China	K	Sino-Korean C	123	*Tectons*				
Liaoning 50	China	K	Sino-Korean C	200	Elliot County	N. America	K	Grenville O	15
Liaoning 51	China	K	Sino-Korean C	18	The Thumb	N. America	UML	Laurentian O	11
Shengli 1	China	K	Sino-Korean C	41	Dongfanghong	China	B	Sino-Korean C	7
Aries	Australia	K	N. Australia C	25	Gansu	China	B	Sino-Korean C	18
Bow Hill	Australia	K	N. Australia C	24	Liulin	China	K?	Sino-Korean C	25
Hadfields Dike	Australia	K	N. Australia C	31	Shexian 4	China	K?	Sino-Korean C	14
Pteropus	Australia	K	N. Australia C	86	Shexian 6	China	K?	Sino-Korean C	19
Seppelt 1	Australia	K	N. Australia C	75	SXBB	China	B	Sino-Korean C	19
Skerring	Australia	K	N. Australia C	18	Teiling 1	China	K?	Sino-Korean C	38
Majhgawan	India	L	Arivalli C	161	Teiling 20	China	K?	Sino-Korean C	23
Andra Pradesh 7	India	K	Dharwar C	50	White Cliffs	Australia	B	S. Australia C	291
Total	**112**		**11**	**7508**	Malaita	S. Pacific	UML	Ontong–Java Plat.	46
					Total	**13**		**5**	**526**

*A, alluvial; K, kimberlite; L, lamproite; B, basalt; UML, lamprophyre.
†C, craton; O, orogen; FB, fold belt.